Nanostructures Investigated by Small Angle Neutron Scattering

H. Frielinghaus

This document has been published in

Thomas Brückel, Gernot Heger, Dieter Richter, Georg Roth and Reiner Zorn (Eds.):
Lectures of the JCNS Laboratory Course held at Forschungszentrum Jülich and the research reactor FRM II of TU Munich
In cooperation with RWTH Aachen and University of Münster
Schriften des Forschungszentrums Jülich / Reihe Schlüsseltechnologien / Key Technologies, Vol. 39
JCNS, RWTH Aachen, University of Münster
Forschungszentrum Jülich GmbH, 52425 Jülich, Germany, 2012
ISBN: 978-3-89336-789-4

5 Nanostructures Investigated by Small Angle Neutron Scattering

H. Frielinghaus
Jülich Centre for Neutron Science
Forschungszentrum Jülich GmbH

Contents

Lecture Notes of the JCNS Laboratory Course Neutron Scattering

5.1 Introduction

Small angle neutron scattering aims at length scales ranging from nanometers to micrometers [1, 2]. This is the typical mesoscale where often atomistic properties can be neglected but structurally systems self-organize, i.e. self-assemble. The structural information about the mesoscale is therefore indispensible for the understanding of the macroscopic behavior. Fundamental concepts of many materials are verified by small angle neutron scattering which supports the finding of new materials for the future. Especially for formulations with many substances, the individual role of each of them is often unclear. The use of theoretical models helps to understand the mechanism of additives. Using these concepts, the system behavior for remote parameter ranges can be predicted which overcomes tedious trial and error concepts.

The simplest molecules which leave the atomistic scale are chain like. Model polymers chemically string identical monomers linearly. These macromolecules have a lot of internal degrees of freedom which practically leads to the formation of coils. Studying the structure of these coils is a typical application for small angle neutron scattering. In this way, the coil size can be related to the monomer structure. The high entropy of polymers is responsible for rubber elasticity. The deformation of polymers under stress is an important question of nowadays research. The often used solid filler particles complicate the physical behavior of the polymers and not all details are finally understood. The larger particles strengthen the mechanical behavior, but there are also nanoparticles which cause the opposite behavior.

Proteins are important building blocks of biological systems. Often, they are characterized as crystals by x-ray scattering. These structures are roughly corresponding to the natural state, but often specific properties cannot be explained completely. It is known that the aqueous environment changes the structure of proteins. The parallel structural characterization of dissolved proteins in water is a typical application for small angle neutron scattering. Another point of criticism is the dynamics of proteins. While the crystalline structures are rather rigid and do not reflect the highly dynamical properties, the dissolved proteins include such effects. In combination with neutron spin echo spectroscopy aiming at the dynamics explicitly the fluctuations of protein shapes are also explained on the basis of small angle neutron scattering experiments. All these details explain the function of proteins in their natural environment of biological systems.

When molecules include groups which tend to separate often microdomains are formed. While macroscopic phase separation is inhibited the self-organization of the molecules leads to highly ordered structures. Examples are liquid crystals – more generally one speaks of liquid crystalline order. The microdomains are again of nanometer size and are well characterized by small angle neutron scattering. Aligned single crystals and 'powder' samples are also of interest. Important questions range from optical to mechanical properties.

Membranes represent the field of surface science. In biology, many questions arise about the function of cell membranes. The major molecules are lipids with a hydrophilic head and a hydrophobic tail. These molecules form bilayers with the hydrophobic moiety in the middle. The bilayer has a thickness of a few nanometers and, thus, fits perfectly to small angle neutron scattering. On larger scales the membranes form closed vesicles or membrane stacks for example. Biologically embedded proteins and smaller molecules such as cholesterol enrich the behavior of the simple membranes. While these examples are rather biologically motivated, surfactant molecules resemble the lipids, but are often used as soaps and detergents. A microemulsion dissolves oil and water macroscopically by adding certain amounts surfactant. Microscopically, oil and water stay demixed and form microdomains which ideally suit the length scales of a neutron small angle scattering experiment. Certain polymers as additives allow for increasing the surfactant efficiency dramatically. This application is environmentally friendly and saves resources.

So small angle neutron scattering experiments connect fundamental physics with chemical and biological aspects and finally lead to industrial applications. May the reader find enlightening ideas for new applications of small angle neutron scattering.

5.2 Survey about the SANS technique

At the research reactor FRM 2 in Garching, the neutron radiation is used for experiments. In many cases, materials are examined in terms of structure and dynamics. The word neutron radiation already contains the wave-particle duality, which can be treated theoretically in quantum mechanics. By neutron we mean a corpuscle usually necessary for the construction of heavier nuclei. The particle properties of the neutron become visible when classical trajectories are describing the movement. The equivalent of light is obtained in geometrical optics, where light rays are described by simple lines, and are eventually refracted at interfaces. However, for neutrons the often neglected gravity becomes important. A neutron at a (DeBroglie) wavelength of 7Å ($= 7 \times 10^{-10}$m) has a velocity of $v = h/(m_n\lambda) = 565$m/s. Over a distance of 20m this neutron is therefore falling by 6.1mm. Thus, the design of neutron instruments is oriented to straight lines with small gravity corrections. Only very slow neutrons show significant effects of gravitation, such as the experiment of H. Meier-Leibnitz described at the subway station 'Garching Forschungszentrum'. The wave properties of neutrons emerge when there is an interaction with materials and the structural size is similar to the neutron wavelength. For the neutron wavelength 7Å these are about 5 atomic distances of carbon. For a Small Angle Neutron Scattering (SANS) experiment we will see that the typical structural sizes investigated are in the range of 20 to 3000Å. The coherence of the neutron must, therefore, be sufficient to examine these structural dimensions. Classically, this consideration will be discussed in terms of resolution (see below). The scattering process appears only due to the wave properties of the neutron.

A scattering experiment is divided into three parts. First, the neutrons are prepared with regard to wavelength and beam alignment. The intensity in neutron experiments is much lower than in experiments with laser radiation or x-rays at the synchrotron. Therefore, an entire wavelength band is used, and the divergence of the beam is limited only as much as necessary. The prepared beam penetrates the sample, and is (partly) scattered. For every neutron scattering experiment elastic and inelastic scattering processes occur. The typical length scales of small angle scattering focus on the nanometer (up to micrometer). The corresponding movements of such large volumes are slow and the scattering processes are called quasi elastic in this Q-range. For simplicity, we assume elastic scattering processes as the idealized condition. So, there is virtually no energy transferred to the neutron. However, the direction changes in the scattering process. The mean wave vector of the prepared beam $\mathbf{k}_i$ (with $|\mathbf{k}_i| = 2\pi/\lambda$) is deflected according to the scattering process to the final wave vector $\mathbf{k}_f$. The scattered neutrons are detected with an area detector. The experimental information is the measured intensity as a function of the solid

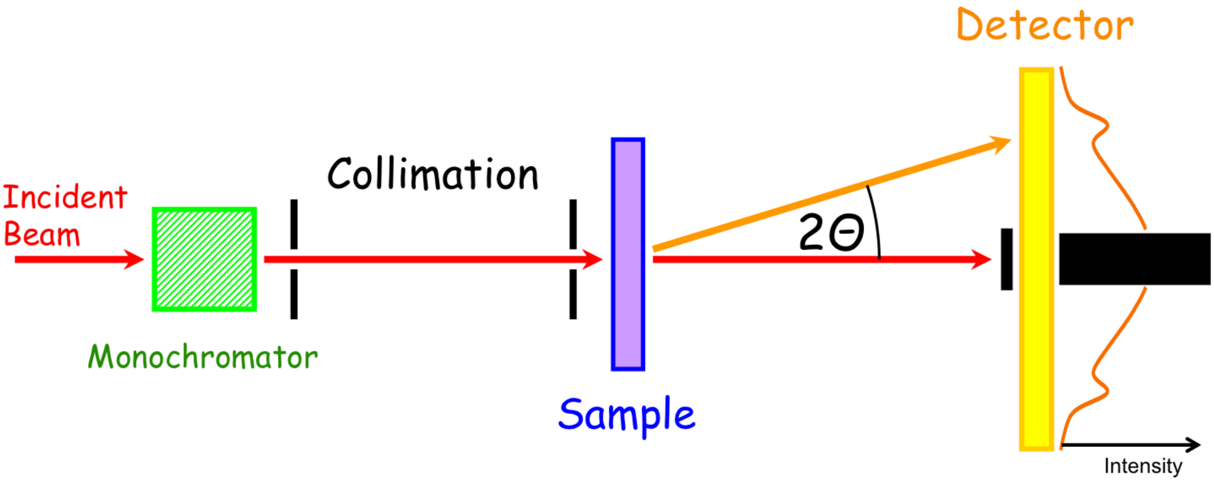

Fig. 5.1: *Scheme of a small angle neutron scattering instrument. The neutrons pass from the left to the right. The incident beam is monochromated and collimated before it hits the sample. Non-scattered neutrons are absorbed by the beam stop in the center of the detector. The scattered neutron intensity is detected as a function of the scattering angle 2θ.*

angle Ω. This solid angle is defined relatively to an ideally small sample and for large detector distances.

In practice, the classical small-angle neutron scattering apparatus including the source looks like this: In the reactor a nuclear chain reaction takes place. A uranium nucleus ^{235}U captures a free neutron, and fission to smaller nuclei takes place. Additionally, 2.5 neutrons (on average) are released, which are slowed down to thermal energy by the moderator. One part of the neutrons keeps the chain reaction going, while the remaining part can be used for neutron experiments. The cold source is another moderator, which cools the neutrons to about 30K. Here, materials with light nuclei (deuterium at FRM 2) are used to facilitate the thermalization. The cold neutrons can easily be transported to the instruments by neutron guides. Rectangular glass tubes are used with a special mirror inside. The neutron velocity selector works mechanically (Fig. 5.1 shows scheme). A rotating cylinder with tilted lamellae allows only neutrons with a certain speed to pass (Fig. 5.2). The wavelengths distribution is ideally triangular with a relative half-width of $\pm 5\%$ or $\pm 10\%$. The collimation determines the divergence of the beam. The entrance aperture and the sample aperture have a distance L_C, and restrict the divergence of the beam. The sample is placed directly behind the sample aperture (Fig. 5.3). Many unscattered neutrons leave the sample and will be blocked by an absorber at the front of the detector. Only the scattered neutrons are detected by the detector at a distance L_D. The sensitive detector detects about 93% of the scattered neutrons, but the huge primary beam cannot be handled, and, therefore, is absorbed by an absorber. In the instruments KWS-1 and KWS-2, the beam stop contains a small counter to measure the unscattered neutrons in parallel. The classic small-angle neutron scattering apparatus is also known as pinhole camera, because the entrance aperture is imaged to the detector by the sample aperture. The sample aperture may be opened further if focusing elements maintain (or improve) the quality of the image of the entrance aperture. By focusing elements the intensity of the experiment may be increased on the expense of needing large samples. Focusing elements can be either curved mirrors or neutron lenses made of MgF_2. Both machines KWS-1 & KWS-2 have neutron lenses, but for this lab course they will not be used.

5.2.1 The scattering vector Q

In this section, the scattering vector $\mathbf{Q}$ is described with its experimental uncertainty. The scattering process is schematically shown in Fig. 5.4, in real space and momentum space. In real space the beam hits the sample with a distribution of velocities (magnitude and direction). The neutron speed is connected to the wavelength, whose distribution is depending on the velocity selector. The directional distribution is defined by the collimation. After the scattering process, the direction of the neutron is changed, but the principal inaccuracy remains the same. The scattering angle 2θ is the azimuth angle. The remaining polar angle is not discussed further here. For samples with no preferred direction, the scattering is isotropic and, thus, does not depend on the polar angle. In reciprocal space, the neutrons are defined by the wave vector $\mathbf{k}$. The main direction of the incident beam is defined as the z-direction, and the modulus is determined by the wavelength, so $|\mathbf{k}_i| = 2\pi/\lambda$. Again, $\mathbf{k}$ is distributed due to the selector and the collimation inaccuracies. The wave vector of the (quasi) elastic scattering process has the same modulus, but differs in direction, namely by the angle 2θ. The difference between both wave vectors is given by the following value:

$$Q = \frac{4\pi}{\lambda}\sin\theta \tag{5.1}$$

For isotropic scattering samples, the measured intensity depends only on the absolute value of the scattering vector $Q = |\mathbf{Q}|$. For small angles, the common approximation of small angle (neutron) scattering is valid:

$$Q = \frac{2\pi}{\lambda}\cdot 2\theta \tag{5.2}$$

The typical Q-range of a small angle scattering instrument thus follows from the geometry. The detector distances L_D vary in the range from 1m to 20m. The area detector is active between $\varnothing_D = 2$cm and 35cm from the center. The angle 2θ is approximated by the ratio $\varnothing_D/L_D$ and the wavelength λ varies between 4.5 and 20Å (typically 7Å). For the instruments KWS-1 and KWS-2, a typical Q-range from 10^{-3} to 0.6Å^{-1} is obtained.

The Q-vector describes which length scales ℓ are observed, following the rule $\ell = 2\pi/Q$. If a Bragg peak is observed, the lattice parameters can be taken directly from the position of the peak. If the scattering shows a sudden change at a certain Q-value, we obtain the length scale of the structural differences. There are characteristic scattering behaviors that can be described by so called scattering laws that are simple power laws Q^α with different exponents α.

5.2.2 The Fourier transformation in the Born approximation

This section deals with the physical explanation for the appearance of the Fourier transformation in the Born approximation. In simple words, in a scattering experiment one observes the intensity as the quadrature of the Fourier amplitudes of the sample structure. This is considerably different from microscopy where a direct image of the sample structure is obtained. So the central question is: Where does the Fourier transformation come from?

Fig. 5.2: *The neutron velocity selector of the small angle scattering instrument KWS-3 at the research reactor Garching FRM-2. This selector was especially manufactured for larger wavelengths (above 7Å).*

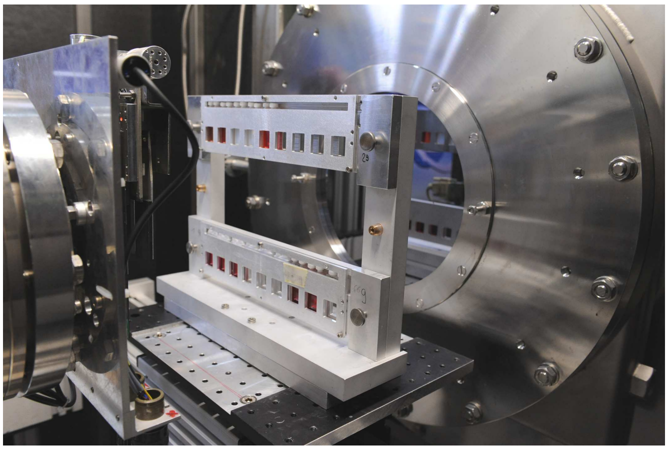

Fig. 5.3: *View on the sample position of the small angle scattering instrument KWS-1 at the research reactor Garching FRM-2. The neutrons come from the left through the collimation and sample aperture (latter indicated). A sample changer allows for running 27 samples (partially colored solutions) in one batch file. The silicon window to the detector tube is seen behind.*

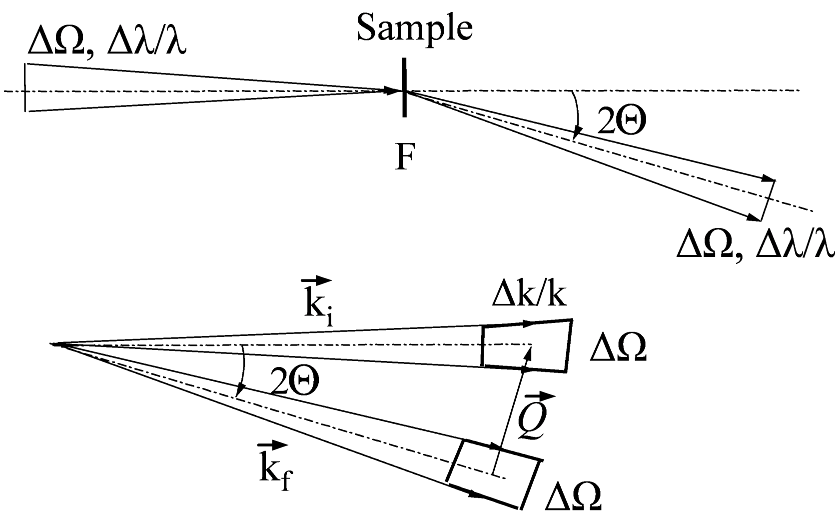

Fig. 5.4: Above: *the neutron speed and its distribution in real space, before and after the scattering process.* Bottom: *The same image expressed by wave vectors (reciprocal space). The scattering vector is the difference between the outgoing and incoming wave vector.*

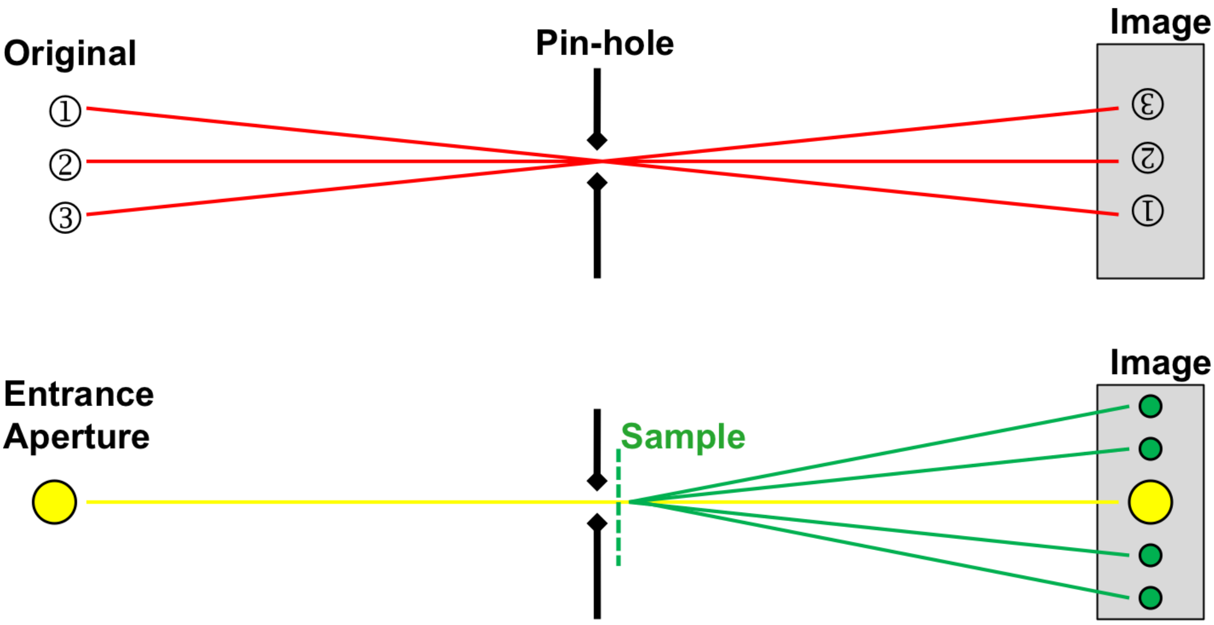

Fig. 5.5: *The principle of a pin-hole camera transferred to the pin-hole SANS instrument.* Top: *The pin-hole camera depicts the original image (here consisting of three numbers). For simplicity, the three points are represented by three rays which meet in the pin-hole, and divide afterwards. On the screen, a real space image is obtained (upside down).* Bottom: *The pin-hole SANS instrument consists of an entrance aperture which is depicted on the detector through the pin-hole (same principle as above). The sample leads to scattering. The scattered beams are shown in green.*

The classical SANS instruments are also called pin-hole instruments. Historically, pin-hole cameras were discovered as the first cameras. They allowed to picture real sceneries on blank screens – maybe at different size, but the image resembled the original picture. The components of this imaging process are depicted in Fig. 5.5. Let's assume the following takes place with only one wavelength of light. The original image is then a monochromatic picture of the three numbers 1, 2 and 3. The corresponding rays meet in the pin-hole, and divide afterwards. On the screen, the picture is obtained as a real-space image, just appearing upside down. From experience we know that the screen may be placed at different distances resulting in different sizes of the image. The restriction of the three beams through the pin-hole holds for the right space behind the pin-hole. In front of the pin-hole the light propagates also in other directions – it is just absorbed by the wall with the pin-hole.

So far, we would think that nothing special has happened during this process of reproduction. But what did happen to the light in the tiny pin-hole? We should assume that the size of the pin-hole is considerably larger than the wavelength. Here, the different rays of the original image interfere and inside the pin-hole a wave field is formed. The momentum along the optical z-axis indicates the propagation direction, and is not very interesting (because is nearly constant for all considered rays). The momenta in the x-y-plane are much smaller and indicate a direction. They originate from the original picture and remain constant during the whole process. Before and after the pin-hole the rays are separated and the directions are connected to a real-space image. In the pin-hole itself the waves interfere and the wave field looks more complicated. The information about the original scenery is conserved through all the stages. That means that also the wave field inside the pin-hole is directly connected to the original picture.

From quantum mechanics (and optics), we know that the vector of momentum is connected to a wave vector. This relation describes how the waves inside the pin-hole are connected to a spectrum of momenta. In classical quantum mechanics (for neutrons), a simple Fourier transformation describes how a wave field in real space (pin-hole state) is connected with a wave field in momentum space (separated beams). In principle, the interpretation is reversible. For electromagnetic fields (for x-rays), the concept has to be transferred to particles without mass. Overall, this experiment describes how the different states appear, and how they are related. The free propagation of a wave field inside a small volume (pin-hole) leads to a separation of different rays accordingly to their momentum.

Now we exchange the original image by a single source (see yellow spot in lower part of Fig. 5.5). This source is still depicted on the image plate (or detector). If we insert a sample at the position of the pin-hole, the wave field starts to interact with the sample. In a simplified way we can say that a small fraction of the wave field takes the real space structure of the sample while the major fraction passes the sample without interaction. This small fraction of the wave field resulting from the interaction propagates freely towards the image plate and generates a scattering pattern. As we have learned, the momenta present in the small fraction of the wave field give rise to the separation of single rays. So the real space image of the sample leads to a Fourier transformed image on the detector. This is the explanation, how the Fourier transformation appears in a scattering experiment – so this is a simplified motivation for the Born approximation. A similar result was found by Fraunhofer for the diffraction of light at small apertures. Here, the aperture is impressed to the wave field (at the pin-hole), and the far field is connected to the Fourier transformation of the aperture shape.

Later, we will see that the size of wave field packages at the pin-hole is given by the coherence volume. The scattering appears independently from such small sub-volumes and is a simple superposition.

5.2.3 Remarks on focusing instruments

We have described the resolution function of the pin-hole SANS instrument very well. This design comes to its limits if very large structures (of $\sim$ μm) need to be resolved. Usually focusing instruments take over because they provide higher intensities at higher resolutions.

Focusing instruments have the same motivation as photo cameras. When the pin-hole camera does not provide proper intensities any more, focusing elements – such as lenses – allow for opening the apertures. Then the resolution is good while the intensity increases to a multiple of its original value. For focusing SANS instruments this means that the sample sizes must be increased accordingly to the lens or mirror size.

There are two possible ways for focusing elements: Neutron lenses are often made of MgF_2. Large arrays of lenses take an overall length of nearly one meter. This is due to the low refractive index of the material for neutrons. A disadvantage of the lenses is the dispersion relation which leads to strong chromatic aberrations. So it is hardly possible to focus the full wavelength band of classical neutron velocity selectors on the detector. Other ways like magnetic neutron lenses have to deal with similar problems.

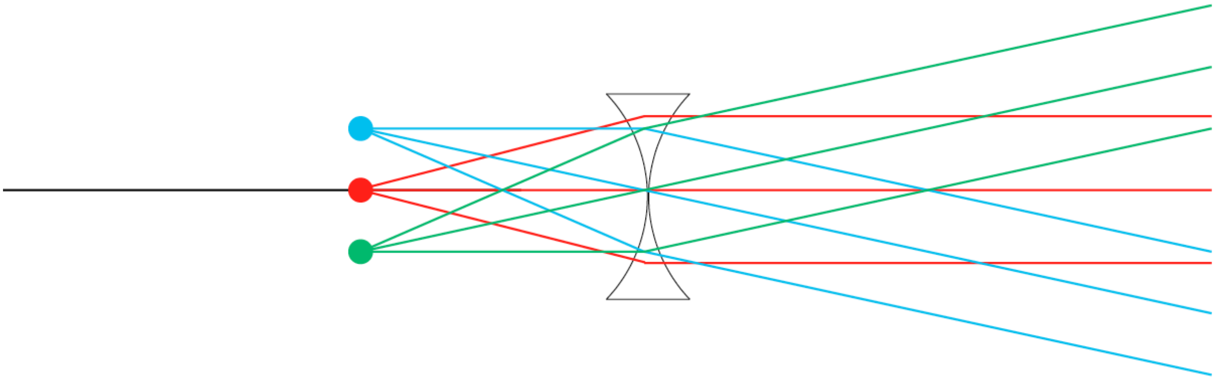

Fig. 5.6: *How a Fourier transformation is obtained with refractive lenses. The real space structure in the focus of the lens is transferred to differently directed beams. The focusing lens is concave since for neutrons the refractive index is smaller than 1.*

The focusing mirror does not show chromatic aberration. So this focusing element provides the highest possible resolution at highest intensities. The small angle scattering instrument KWS-3 is a unique instrument which uses this technique. The mirror technique was motivated by satellite mirrors. The roughness needs to stay below a few Ångström over large areas.

Practically the entrance aperture may be closed to a few millimeters while the sample aperture takes a few square centimeters accordingly to the mirror size. This setup images the entrance aperture on the detector. So, the primary beam profile has sharp edges in comparison to the triangular shapes of the pin-hole camera. This narrower distribution of intensity means that the beam stop might be slightly smaller than for a similar pin-hole instrument and so the focusing instrument improves the intensity-resolution problem by a rough factor of two.

For a symmetric set-up (collimation and detector distance equal, i.e. $L_C = L_D$) the focusing optic is in the middle at the sample position. The focus f is half the collimation distance, i.e. $f = \frac{1}{2}L_C = \frac{1}{2}L_D$. Now the places where exact Fourier transforms are obtained (from the entrance aperture and from the sample structure) do not agree anymore. The sample is still considered as a small volume and from there the waves propagate freely to the detector, and the already known relation between sample structure and scattering image holds.

For focusing elements, the places of Fourier transformations differ (see Fig. 5.6). The original structure is placed in the focus, and the resulting distinctive rays are obtained at the other side of the lens in the far field. So for focusing SAS instruments, the places of appearing Fourier transformations for the entrance aperture and the sample structure differ.

The historical development of cameras can be seen in parallel. The first cameras were pin-hole cameras, but when lenses could be manufactured lens cameras replaced the old ones. The direct advantage was the better light yield being proportional to the lens size. Another effect appeared: The new camera had a depth of focus – so only certain objects were depicted sharply, which was welcomed in the art of photography. The focusing SAS instrument depicts only the entrance aperture, and the focusing is not a difficult task. The higher intensity or the better resolution are the welcomed properties of the focusing SAS instrument.

5.2.4 Measurement of the macroscopic cross section

In this section, the macroscopic scattering cross section is connected to the experimentally measured intensity. The experimental intensity is dependent on the instrument at hand, while the macroscopic scattering cross section describes the sample properties independent of instrumental details. The absolute calibration allows to compare experimental data between different measurements. In theory, the intensity and the cross section are connected by:

$$\frac{\Delta I}{\Delta\Omega}(\mathbf{Q}) = I_0 \cdot A \cdot T_r \cdot t \cdot \frac{d\Sigma}{d\Omega}(\mathbf{Q}) \tag{5.3}$$

The intensity ΔI for one detector channel is measured as a function of the scattering angle. Each detector channel covers the solid angle $\Delta\Omega$. The experimental intensity is proportional to: (a) the intensity at the sample position I_0 (in units of neutrons per second per area), (b) of the irradiated area A, (c) the transmission of the sample (the relative portion of non-scattered neutrons), (d) of the sample thickness t, and (e) the macroscopic scattering cross section $d\Sigma/d\Omega$. In most practical cases, the primary intensity cannot be detected by the same detector. By a calibration measurement of a substance with known scattering strength the primary intensity is measured indirectly. At KWS-1 and KWS-2 we often use plexiglass, which scatters only incoherently (due to the hydrogen content). The two measurements under the same conditions will be put in relation, which thereby eliminates the identical terms. One writes:

$$\frac{\left.\frac{\Delta I(\mathbf{Q})}{\Delta\Omega}\right|_{\text{sample}}}{\left.\frac{\Delta I(\mathbf{Q})}{\Delta\Omega}\right|_{\text{plexi}}} = \frac{I_0 \cdot A \cdot T_{r,\text{sample}} \cdot t_{\text{sample}}}{I_0 \cdot A \cdot T_{r,\text{plexi}} \cdot t_{\text{plexi}}} \cdot \frac{\left.\frac{d\Sigma(\mathbf{Q})}{d\Omega}\right|_{\text{sample}}}{\left.\frac{d\Sigma(\mathbf{Q})}{d\Omega}\right|_{\text{plexi}}} \tag{5.4}$$

The macroscopic scattering cross section of the plexiglass measurement does not depend on the scattering vector. The measured intensity of the plexiglass is also a measure of the detector efficiency, as different channels can have different efficiency. The plexiglass specific terms are merged to $\mu_{\text{plexi}} = T_{r,\text{plexi}} \cdot t_{\text{plexi}} \cdot (d\Sigma/d\Omega)_{\text{plexi}}$. So, finally the macroscopic scattering cross-section reads:

$$\left.\frac{d\Sigma(\mathbf{Q})}{d\Omega}\right|_{\text{sample}} = \frac{\mu_{\text{plexi}}}{T_{r,\text{sample}} \cdot t_{\text{sample}}} \frac{\Delta I(\mathbf{Q})|_{\text{sample}}}{\Delta I(\mathbf{Q})|_{\text{plexi}}} \cdot \left(\frac{L_{D,\text{sample}}}{L_{D,\text{plexi}}}\right)^2 \tag{5.5}$$

Essentially, formula 5.5 follows directly from equation 5.4. The last factor results from the solid angles of the two measurements, which in principle can be done at different detector distances L_D. Plexiglass is an incoherent scatterer, and therefore can be measured at smaller detector distances to obtain an increased intensity. Nonetheless, the collimation setting must be the same as for the sample measurement.

5.2.5 Incoherent background

The macroscopic cross section usually has two contributions: the coherent and incoherent scattering. For small angle neutron scattering the incoherent scattering is mostly Q-independent and does not contain important information:

$$\left.\frac{d\Sigma}{d\Omega}(\mathbf{Q})\right|_{\text{total}} = \left.\frac{d\Sigma}{d\Omega}(\mathbf{Q})\right|_{\text{coh}} + \left.\frac{d\Sigma}{d\Omega}\right|_{\text{incoh}} \tag{5.6}$$

We therefore tend to subtract the incoherent scattering. It is well determined at large Q when the coherent scattering becomes small. The origin of the incoherent scattering is the spin-dependent scattering length. Especially for hydrogen ^{1}H the neutron spin and the nuclear spin form a singlet or triplet state with different scattering lengths. The average scattering length of these two states contributes to the coherent scattering. The variance of the scattering length gives rise to the incoherent scattering. Here, each of the nuclei appears as an independent point scatterer which in reciprocal space means a Q-independent scattering signal. The dependence of the scattering on the neutron spin means that neutron spin polarization and analysis yields another method to determine the incoherent scattering independently from the coherent signal.

5.2.6 Resolution

The simple derivatives of equation 5.2 support a very simple view on the resolution of a small angle neutron scattering experiment. We obtain:

$$\left(\frac{\Delta Q}{Q}\right)^2 = \left(\frac{\Delta\lambda}{\lambda}\right)^2 + \left(\frac{2\Delta\theta}{2\theta}\right)^2 \tag{5.7}$$

The uncertainty about the Q-vector is a sum about the uncertainty of the wavelength and the angular distribution. Both uncertainties result from the beam preparation, namely from the monochromatization and the collimation. The neutron velocity selector selects a wavelength band of either $\pm 5\%$ or $\pm 10\%$. The collimation consists of an entrance aperture with a diameter d_C and a sample aperture of a diameter d_S. The distance between them is L_C.

One property of eq. 5.7 is the changing importance of the two contributions at small and large Q. At small Q the wavelength spread is nearly negligible and the small terms Q and θ dominate the resolution. This also means that the width of the primary beam is exactly the width of the resolution function. More exactly, the primary beam profile describes the resolution function at small Q. Usually, the experimentalist is able to change the resolution at small Q. At large Q the resolution function is dominated by the wavelength uncertainty. So the experimentalist wants to reduce it – if possible – for certain applications. This contribution is also an important issue for time-of-flight SANS instruments at spallation sources. The wavelength uncertainty is determined by the pulse length of the source and cannot be reduced without intensity loss.

A more practical view on the resolution function includes the geometrical contributions explicitely [3]. One obtains:

$$\left(\frac{\sigma_Q}{Q}\right)^2 = \frac{1}{8\ln 2}\left(\left(\frac{\Delta\lambda}{\lambda}\right)^2 + \left(\frac{1}{2\theta}\right)^2 \cdot \left[\left(\frac{d_C}{L_C}\right)^2 + d_S^2\left(\frac{1}{L_C}+\frac{1}{L_D}\right)^2 + \left(\frac{d_\mathrm{D}}{L_D}\right)^2\right]\right) \tag{5.8}$$

Now the wavelength spread is described by $\Delta\lambda$ being the full width at the half maximum. The geometrical terms have contributions from the aperture sizes d_C and d_S and the spatial detector resolution d_D. The collimation length L_C and detector distance L_D are usually identical such that all geometric resolution contributions are evenly large ($d_C = 2d_S$ then). This ideal setup maximizes the intensity with respect to a desired resolution.

The resolution function profile is another topic of the correction calculations. A simple approach assumes Gaussian profiles for all contributions, and finally the overall relations read:

$$\left.\frac{d\Sigma(\bar{Q})}{d\Omega}\right|_{\text{meas}} = \int_0^\infty dQ\, R(Q-\bar{Q}) \cdot \left.\frac{d\Sigma(Q)}{d\Omega}\right|_{\text{theo}} \tag{5.9}$$

$$R(Q-\bar{Q}) = \frac{1}{\sqrt{2\pi}\sigma_Q} \exp\left(-\frac{1}{2}\frac{(Q-\bar{Q})^2}{\sigma_Q^2}\right) \tag{5.10}$$

The theoretical macroscopic cross section is often described by a model function which is fitted to the experimental data. In this case the computer program only does a convolution of the model function with the resolution function $R(\Delta Q)$. Alternatively, there are methods to deconvolute the experimental data without modeling the scattering at first hand.

The here described resolution function is given as a Gaussian. This is true for relatively narrow distributions. The reason for using a Gaussian function although the original distributions of λ and θ are often triangular is: The central limit theorem can be applied to this problem because we have seen from eq. 5.8 that there are four contributions to the resolution function, and the radial averaging itself also smears the exact resolution function further out. Thus, the initial more detailed properties of the individual distributions do not matter anymore. Equations 5.9 and 5.10 are a good approximation for many practical cases.

We now want to describe the connection between the resolution function and the coherence of the neutron beam at the sample position. From optics we know about the transverse coherence length:

$$\ell_{\text{coh,transv}} = \frac{\lambda L_C}{2d_C} \qquad \text{is similar to} \qquad \Delta Q_\theta^{-1} = \frac{\lambda L_C}{\pi d_C} \tag{5.11}$$

It can be compared well with the geometric resolution contribution that arises from the entrance aperture only. Small differences in the prefactors we can safely neglect. For the longitudinal coherence length we obtain:

$$\ell_{\text{coh,long}} = \frac{1}{4}\lambda\left(\frac{\Delta\lambda}{\lambda}\right)^{-1} \qquad \text{is similar to} \qquad \Delta k^{-1} = \frac{1}{2\pi}\lambda\left(\frac{\Delta\lambda}{\lambda}\right)^{-1} \tag{5.12}$$

This coherence length can be well compared to the wavevector uncertainty of the incoming beam. If we look back on Figure 5.4 we see that the coherence volume exactly describes the uncertainty of the incoming wave vector. The two contributions are perpendicular which supports the vectorial (independent) addition of the contributions in eq. 5.8 for instance. The coherence volume describes the size of the independent wave packages which allow for wave-like properties such as the scattering process. So the coherence volume describes the maximum size

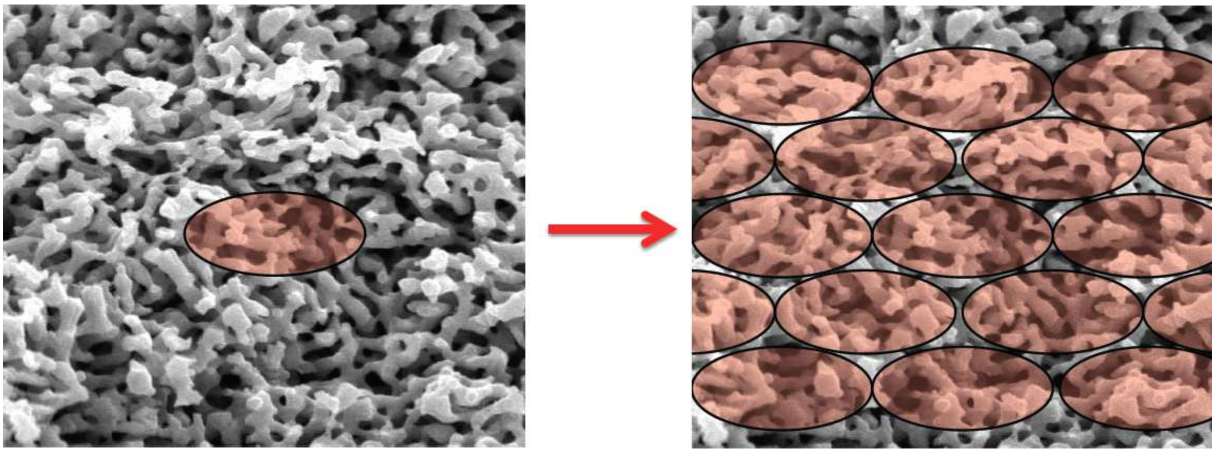

Fig. 5.7: *The coherence volume is usually much smaller than the sample volume (left). So the overall scattering appears as an incoherent superposition of the scattering from many coherence volumes (right).*

of structure that is observable by SANS. If larger structures need to be detected the resolution must be increased.

The understanding how the small coherence volume covers the whole sample volume is given in the following (see also Fig. 5.7). Usually the coherence volume is rather small and is many times smaller than the irradiated sample volume. So many independent coherence volumes cover the whole sample. Then, the overall scattering intensity occurs as an independent sum from the scattering intensities of all coherence volumes. This is called incoherent superposition.

5.3 The theory of the macroscopic cross section

We have seen that the SANS instrument aims at the macroscopic cross section which is a function of the scattering vector $\mathbf{Q}$. In many examples of isotropic samples and orientationally averaged samples (powder samples) the macroscopic cross section depends on the modulus $|\mathbf{Q}| \equiv Q$ only. This measured function has to be connected to important structural parameters of the sample. For this purpose model functions are developed. The shape of the model function in comparison with the measurement already allows to distinguish the validity of the model. After extracting a few parameters with this method, deeper theories – like thermodynamics – allow to get deeper insight about the behavior of the sample. Usually, other parameters – like concentration, temperature, electric and magnetic fields, ... – are varied experimentally to verify the underlying concepts at hand. The purpose of this section is to give some ideas about model functions.

When the Born approximation was developed several facts and assumptions came along. The scattering amplitudes of the outgoing waves are derived as perturbations of the incoming plane wave. The matrix elements of the interaction potential with these two wave fields as vectors describe the desired amplitudes. The interaction potential can be simplified for neutrons and the nuclei of the sample by the Fermi pseudo potential. This expresses the smallness of the nuclei ($\sim$1fm) in comparison to the neutron wavelength ($\sim$Å). For the macroscopic cross section we immediately obtain a sum over all nuclei:

$$\frac{d\Sigma}{d\Omega}(\mathbf{Q}) = \frac{1}{V}\left|\sum_j b_j \exp(\mathrm{i}\mathbf{Q}\cdot\mathbf{r}_j)\right|^2 \tag{5.13}$$

This expression is normalized to the sample volume V because the second factor usually is proportional to the sample size. This simply means: The more sample we put in the beam the more intensity we obtain. The second factor is the square of the amplitude because we measure intensities. While for electromagnetic fields at low frequencies one can distinguish amplitudes and phases (without relying on the intensity) the neutrons are quantum mechanical particles where experimentally such details are hardly accessible. For light (and neutrons) for instance holographic methods still remain. The single amplitude is a sum over each nucleus j with its typical scattering length b_j and a phase described by the exponential. The square of the scattering length b_j^2 describes a probability of a scattering event taking place for an isolated nucleus. The phase arises between different elementary scattering events of the nuclei for the large distances of the detector. In principle, the scattering length can be negative (for hydrogen for instance) which indicates an attractive interaction with a phase π. Complex scattering lengths indicate absorption. The quadrature of the amplitude can be reorganized:

$$\frac{d\Sigma}{d\Omega}(\mathbf{Q}) = \frac{1}{V}\sum_{j,k} b_j b_k \exp\left(\mathrm{i}\mathbf{Q}(\mathbf{r}_j - \mathbf{r}_k)\right) \tag{5.14}$$

Here we find then self-terms with identical indices j and k without any phase and cross terms with phases arising from distances between different nuclei. Here it becomes obvious that only relative positions of the nuclei matter which is a result of the quadrature. The overall phase of the sample does not matter because of the modulus in eq. 5.13. We will use this expression for the polymer scattering.

Apart from this detailed expression a simplified view is allowed for small angle scattering experiments. Firstly, we know that the wavelength is typically 7Å which is much larger than the atom-atom distance of ca. 1.5Å. Secondly, the SANS experiment aims at structures at the nanoscale. So the scattering vector aims at much larger distances compared to the atomistic distances (i.e. $2\pi Q^{-1} \gg 1$Å). This allows for exchanging sums by integrals as follows:

$$\sum_j b_j \cdots \quad \longrightarrow \quad \int_V d^3r\ \rho(\mathbf{r}) \cdots \tag{5.15}$$

Such methods are already known for classical mechanics, but reappear all over physics. The meaning is explained by the sketch of Figure 5.8. The polymer polyethylene oxide (PEO) contains many different nuclei of different species (hydrogen, carbon and oxide). However, the SANS method does not distinguish the exact places of the nuclei. The polymer appears rather like a homogenous worm. Inside, the worm has a constant scattering length density which reads:

$$\rho_{\mathrm{mol}} = \frac{1}{V_{\mathrm{mol}}} \sum_{j\in\{\mathrm{mol}\}} b_j \tag{5.16}$$

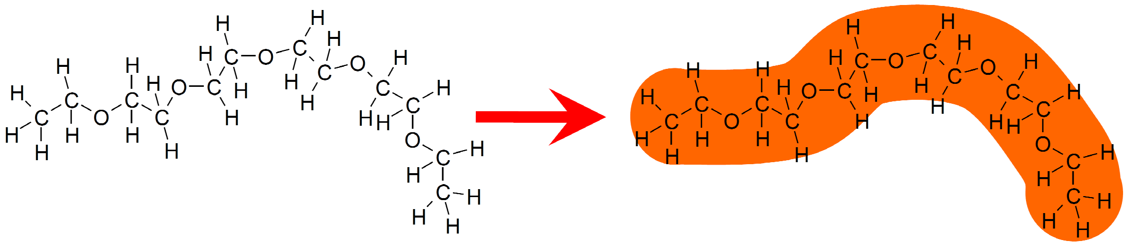

Fig. 5.8: *The concept of the scattering length density. On the left the atomic structure of a polyethylene oxide polymer (PEO) is depicted. For small angle scattering the wavelength is much larger than the atomic distance. So for SANS the polymer appears like a worm with a constant scattering length density inside.*

So, for each molecule we consider all nuclei and normalize by the overall molecule volume. Of course different materials have different scattering length densities ρ. The initial equation 5.13 reads then:

$$\frac{d\Sigma}{d\Omega}(\mathbf{Q}) = \frac{1}{V}\left|\int_V d^3r\ \rho(\mathbf{r})\exp(\mathrm{i}\mathbf{Q}\mathbf{r})\right|^2 \tag{5.17}$$

$$= \frac{1}{V}\left|\mathcal{F}\left[\rho(\mathbf{r})\right]\right|^2 = \frac{1}{V}\left|\rho(\mathbf{Q})\right|^2 \tag{5.18}$$

The single amplitude is now interpreted as a Fourier transformation of the scattering length density $\rho(\mathbf{r})$ which we simply indicate by $\rho(\mathbf{Q})$. The amplitude simply is defined by:

$$\rho(\mathbf{Q}) = \int_V d^3r\ \rho(\mathbf{r})\exp(\mathrm{i}\mathbf{Q}\mathbf{r}) \tag{5.19}$$

Again, equation 5.17 loses the phase information due to the modulus. While we focused on the scattering experiment so far, another view on this function will provide us with further insight. We define the correlation Γ as follows:

$$\Gamma(\mathbf{Q}) = \frac{1}{V}\left|\rho(\mathbf{Q})\right|^2 = \frac{1}{V}\rho^*(\mathbf{Q})\rho(\mathbf{Q}) = \frac{1}{V}\rho(-\mathbf{Q})\rho(\mathbf{Q}) \tag{5.20}$$

The modulus is usually calculated via the complex conjugate $\rho^*(\mathbf{Q})$ which in turn can be obtained by changing the sign of the argument $\mathbf{Q}$. Now the correlation function is a simple product of two Fourier transformed functions. They can be interpreted on the basis of a convolution in real space:

$$\Gamma(\mathbf{r}) = \frac{1}{V}\rho(\mathbf{r}) \otimes \rho(\mathbf{r}) = \frac{1}{V}\int_V d^3r'\ \rho(\mathbf{r}+\mathbf{r}') \cdot \rho(\mathbf{r}') \tag{5.21}$$

The underlying correlation function $\Gamma(\mathbf{r})$ arises from the convolution of the real space scattering length density with itself. The mathematical proof is carried out in Appendix A. For imagining

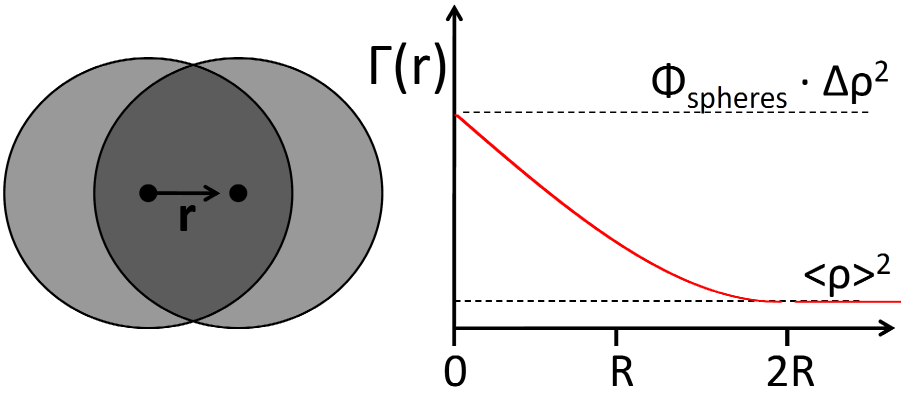

Fig. 5.9: *On the left the meaning of the convolution is depicted. Two identical shapes are displaced by a vector* $\mathbf{r}$. *The convolution volume is the common volume (dark grey). This consideration leads for three-dimensional spheres to the linear correlation function* $\Gamma(\mathbf{r})$ *shown on the right.*

the convolution assume you have two foils with the same pattern printed on. The vector $\mathbf{r}$ describes the relative displacement of the two foils. Then you calculate the product of the two patterns and integrate over V. For patterns of limited size it becomes clear that the function turns to 'zero' at a finite distance $\mathbf{r}$. For simple compact patterns the function monotonically decays. The example of spheres is depicted in Fig. 5.9. In the left the meaning of the convolution is indicated. The darkest area in the center is the considered volume of the convolution for the vector $\mathbf{r}$. In three dimensions this consideration leads to the correlation function (see also Appendix A and references [4, 5]):

$$\Gamma(\mathbf{r}) = \phi_{\text{spheres}} \cdot \Delta\rho^2 \cdot \left\{ \begin{array}{ll} 1 - \frac{3}{2}|\mathbf{r}|/(2R) + \frac{1}{2}|\mathbf{r}|^3/(2R)^3 & \text{for } |\mathbf{r}| \leq 2R \\ 0 & \text{for } |\mathbf{r}| > 2R \end{array} \right\} + \langle\rho\rangle^2 \tag{5.22}$$

The concentration ϕ_{spheres} accounts for many independent, but diluted spheres. The value $\Delta\rho$ is the scattering length density difference between the sphere and the surrounding matrix (i.e. solvent). The constant $\langle\rho\rangle^2$ is the average scattering length density of the overall volume. Apart from these simple rationalizations we can formally calculate the limits for small and large distances $\mathbf{r}$:

$$\Gamma(\mathbf{r} \to 0) = \langle\rho^2\rangle \qquad \Gamma(\mathbf{r} \to \infty) = \langle\rho\rangle^2 \tag{5.23}$$

At this stage the reasons for the limits are based on mathematics. The brackets $\langle\cdots\rangle$ indicate an averaging of a locally defined function $\rho^2(\mathbf{r})$, $\rho(\mathbf{r})$ over the whole volume. For small distances the averaging over squares of the scattering length density usually leads to higher values compared to the average being squared afterwards. So the correlation function often is a monotonically decaying function. A very simple realization is given by:

$$\Gamma(\mathbf{r}) = \left\langle \left(\rho - \langle\rho\rangle\right)^2 \right\rangle \exp\left(-|\mathbf{r}|/\xi\right) + \langle\rho\rangle^2 \tag{5.24}$$

The shape of the decay is usually described by an exponential decay and can be motivated further in detail [1]. The first addend is proportional to the fluctuations of the scattering length density. This finding already indicates that scattering experiments are sensitive to fluctuations. The correlation length ξ indicates over which distance the correlations are lost. The current picture does not allow for a complete decay (in comparison to the single sphere which finds $\Gamma(r) = 0$ for $r > 2R$). This means that the current discussion treats scattering length density fluctuations which fill the full 3-dimensional space. The Fourier transformation of eq. 5.24 leads to the following expression:

$$\Gamma(\mathbf{Q}) \propto \left\langle \left(\rho - \langle\rho\rangle\right)^2 \right\rangle \frac{\xi^3}{1 + \xi^2 \mathbf{Q}^2} \tag{5.25}$$

The scattering intensity in this case is proportional to the scattering length density fluctuations, to the coherence volume ξ^3 and the Q-dependent Lorentz peak. The latter has to be interpreted as a kind of expansion. So different details of the decaying correlation function (eq. 5.24) might lead to differently decaying scattering functions. The current Lorentz function is typical for Ornstein-Zernicke correlation functions. Further discussions of the correlation function are given in Appendix A.

For the fluctuations of the scattering length density we would like to consider a two phase system, i.e. the whole space is taken by either component 1 or 2. The concentration of phase 1 is ϕ_1, and the scattering length density is ρ_1 (correspondingly ρ_2 is defined). For the average scattering lenght density we clearly obtain $\langle\rho\rangle = \phi_1\rho_1 + (1-\phi_1)\rho_2$. For the scattering length density fluctuations we obtain similarly $\langle(\rho - \langle\rho\rangle)^2\rangle = \phi_1(1-\phi_1)(\rho_1-\rho_2)^2$. The latter result describes the concentration fluctuations of the two phase system and the scattering length density contrast. For the following considerations the contrast will reappear in many examples.

5.3.1 Spherical colloidal particles

In this section we will derive the scattering of diluted spherical particles in a solvent. These particles are often called colloids, and can be of inorganic material while the solvent is either water or organic solvent. Later in the manuscript interactions will be taken into account.

One important property of Fourier transformations is that constant contributions will lead to sharp delta peaks at $Q = 0$. This contribution is not observable in the practical scattering experiment. The theoretically sharp delta peak might have a finite width which is connected to the overall sample size, but centimeter dimensions are much higher compared to the largest sizes observed by the scattering experiment ($\sim\mu$m). So formally we can elevate the scattering density level by any number $-\rho_{\mathrm{ref}}$:

$$\rho(\mathbf{r}) \longrightarrow \rho(\mathbf{r}) - \rho_{\mathrm{ref}} \qquad \text{leads to} \qquad \rho(\mathbf{Q}) \longrightarrow \rho(\mathbf{Q}) - 2\pi\rho_{\mathrm{ref}}\delta(\mathbf{Q}) \tag{5.26}$$

The resulting delta peaks can simply be neglected. For a spherical particle we then arrive at the simple scattering length density profile:

$$\rho_{\mathrm{single}}(\mathbf{r}) = \begin{cases} \Delta\rho & \text{for } |\mathbf{r}| \leq R \\ 0 & \text{for } |\mathbf{r}| > R \end{cases} \tag{5.27}$$

Inside the sphere the value is constant because we assume homogenous particles. The reference scattering length density is given by the solvent. This function will then be Fourier transformed accordingly:

$$\rho_{\text{single}}(\mathbf{Q}) = \int_0^{2\pi} d\phi \int_0^{\pi} d\vartheta \ \sin\vartheta \int_0^R dr\ r^2\ \Delta\rho\ \exp\left(\mathrm{i}|\mathbf{Q}|\cdot|\mathbf{r}|\cos(\vartheta)\right) \tag{5.28}$$

$$= 2\pi\ \Delta\rho \int_0^R dr\ r^2 \left[\frac{1}{\mathrm{i}Qr}\exp\left(\mathrm{i}QrX\right)\right]_{X=-1}^{X=+1} \tag{5.29}$$

$$= 4\pi\ \Delta\rho \int_0^R dr\ r^2\ \frac{\sin(Qr)}{Qr} \tag{5.30}$$

$$= \Delta\rho\ \frac{4\pi}{3}R^3\left(3\frac{\sin(QR)-QR\cos(QR)}{(QR)^3}\right) \tag{5.31}$$

In the first line 5.28 we introduce spherical coordinates with the vector $\mathbf{Q}$ determining the z-axis for the real space. The vector product $\mathbf{Qr}$ then leads to the cosine term. In line 5.29 the azimutal integral is simply 2π, and the variable $X = \cos\vartheta$ is introduced. Finally, in line 5.30 the kernel integral for spherically symmetric scattering length density distributions is obtained. For homogenous spheres we obtain the final result of eq. 5.31. Putting this result together for the macroscopic cross section (eq. 5.18) we obtain:

$$\frac{d\Sigma}{d\Omega}(\mathbf{Q}) = \frac{N}{V}\cdot\left|\rho_{\text{single}}(\mathbf{Q})\right|^2 = (\Delta\rho)^2\ \phi_{\text{spheres}}\ V_{\text{sphere}}\ F(\mathbf{Q}) \tag{5.32}$$

$$F(\mathbf{Q}) = \left(3\frac{\sin(QR)-QR\cos(QR)}{(QR)^3}\right)^2 \tag{5.33}$$

We considered N independent spheres in our volume V, and thus obtained the concentration of spheres ϕ_{spheres}. Furthermore, we defined the form factor $F(Q)$, which describes the Q-dependent term for independent spheres (or the considered shapes in general). The function is shown in Figure 5.10. The first zero of the form factor is found at $Q = 4.493/R$. This relation again makes clear why the reciprocal space (Q-space) is called reciprocal. We know the limit for small scattering angles is $F(\mathbf{Q}\to 0) = 1 - \frac{1}{5}Q^2R^2$. So the form factor is normalized to 1, and the initial dependence on Q^2 indicates the size of the sphere. For large scattering angles the form factor is oscillating. Usually the instrument cannot resolve the quickest oscillations and an average intensity is observed. The asymptotic behavior would read $F(\mathbf{Q}\to\infty) = \frac{9}{2}(QR)^{-4}$. The obtained power law Q^{-4} is called Porod law and holds for any kind of bodies with sharp interfaces. So, sharp interfaces are interpreted as fractals with $d = 2$ dimensions, and the corresponding exponent is $6 - d$. The general appearance of the Porod formula reads then:

$$\frac{d\Sigma}{d\Omega}(Q) = P\cdot Q^{-4} \tag{5.34}$$

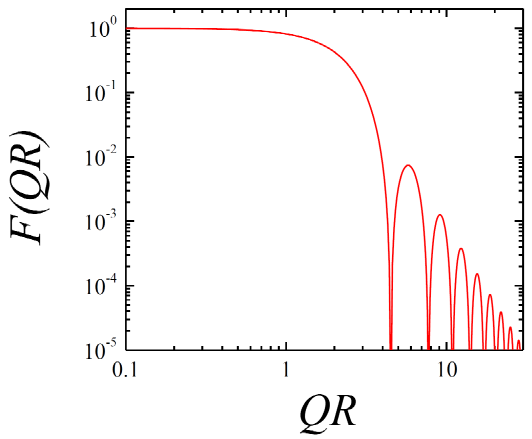

Fig. 5.10: *The form factor of a homogenous sphere in a double logarithmic plot.*

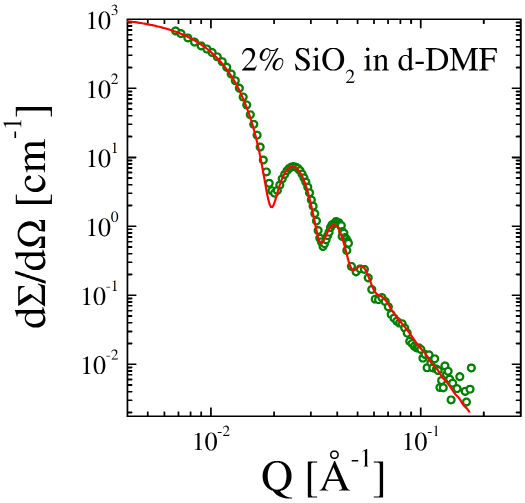

Fig. 5.11: *Experimental scattering curve of spherical SiO_2 colloids in the deuterated solvent DMF [6]. The resolution function (eq. 5.9) is included in the fit (red line).*

The amplitude of the Porod scattering P tells about the surface per volume and reads $P = 2\pi(\Delta\rho)^2 S_{\text{tot}}/V_{\text{tot}}$. Apart from the contrast, it measures the total surface S_{tot} per total volume V_{tot}. For our shperes, the Porod constant becomes $P = 2\pi(\Delta\rho)^2 4\pi R^2/(4\pi R^3/(3\phi)) = 6\pi\phi_1(\Delta\rho)^2/R$. The surface to volume ratio is smaller the larger the individual radius R is. The remaining scaling with the concentration ϕ_1 and the contrast $(\Delta\rho)^2$ arises still from the prefactor which we discussed in context with eq. 5.32.

When comparing the theoretical description of the spherical form factor with measurements one finds a good agreement (Fig. 5.11). Many fringes are seen, but after the third or fourth peak the function does not indicate any oscillation any more. Furthermore, the sharp minima are washed out. All of this is a consequence of the resolution function (eq. 5.9) which has been taken into account for the fitted curve. For many other examples one also needs to take the polydispersity into account. The synthesis of colloids usually produces a whole distribution of different radii. In our example the polydispersity is very low which is the desired case. Polydispersity acts in a similar way compared to the resolution function. The sharp minima are washed out. While the resolution appears as a distribution of different Q-values measured at a certain point the polydispersity integrates over several radii.

Another general scattering law for isolated (dilute) colloids is found for small scattering angles. The general appearance of the Guinier scattering law is:

$$\frac{d\Sigma}{d\Omega}(\mathbf{Q}\to 0) = \frac{d\Sigma}{d\Omega}(0)\cdot\exp\left(-\frac{1}{3}Q^2R_g^2\right) \tag{5.35}$$

When comparing the scattering law of a sphere and the Guinier formula we obtain $R_g = \sqrt{\frac{3}{5}}R$. The radius of gyration R_g can be interpreted as a momentum of inertia normalized to the total mass and specifies the typical size of the colloid of any shape. The Guinier formula can be seen as an expansion at small scattering angles of the logarithm of the macroscopic cross section truncated after the Q^2 term. Further details are discussed in Appendix B.

Another general appearance for independent colloids shall be discussed now using equation 5.32. The macroscopic cross section is determined by several important factors: The contrast between the colloid and the solvent given by $\Delta\rho^2$, the concentration of the colloids, the volume of a single colloid, and the form factor. Especially for small Q the latter factor turns to 1, and the first three factors dominate. When knowing two factors from chemical considerations, the third factor can be determined experimentally using small angle neutron scattering.

When comparing this expression for isolated colloids with the Ornstein-Zernicke result we see in parallel: The contrast stays for both kinds of interpretations. The particle volume corresponds to the correlation volume (i.e. $V \sim \xi^3$). The concentration of the correlation volumes comes close to 1 (i.e. $\phi \sim 1$). Finally, F is a measure for the correlations inside the correlation volume. So, for independent colloids the correlation volume must fully cover the single particle but two neighbored particles are found in distinct correlation volumes. Finally, the overall experimental correlation length is limited by the sample and the radiation coherence. So, for the transversal correlation length one would obtain $\xi_{\mathrm{eff,transv}}^{-2} = \xi^{-2} + \ell_{\mathrm{coh,transv}}^{-2}$.

5.3.2 Contrast variation

For neutron scattering the method contrast variation opens a wide field of possible experiments. For soft matter research the most important labelling approach is the exchange of hydrogen ^{1}H by deuterium ^{2}H. Since in a single experiment the phase information is lost completely the contrast variation experiment retrieves this information partially. Relative positions of two components are obtained by this method.

The scattering length density of the overall sample is now understood to originate from each component individually. So the specific $\rho_j(\mathbf{r})$ takes the value of the scattering length density of component j when the location points to component j and is zero otherwise. We would then obtain the following:

$$\rho(\mathbf{Q}) = \int_V d^3r \left(\sum_{j=1}^{n} \rho_j(\mathbf{r}) \right) \exp(\mathrm{i}\mathbf{Q}\mathbf{r}) \tag{5.36}$$

n specifies the number of components. The assumption of incompressibility means that on every place there is one component present, and so all individual functions $\rho_j(\mathbf{r})$ fill the full space. Furthermore, we would like to define component 1 being the reference component, i.e. $\rho_{\mathrm{ref}} = \rho_1$ (see eq. 5.26). This means that on each place we have a $\Delta\rho_j(\mathbf{r})$ function similar to eq. 5.22. Then, we arrive at:

$$\rho(\mathbf{Q}) = \sum_{j=2}^{n} \Delta\rho_{j1}(\mathbf{Q}) \tag{5.37}$$

The macroscopic cross section is a quadrature of the scattering length density $\rho(\mathbf{Q})$, and so we arrive at:

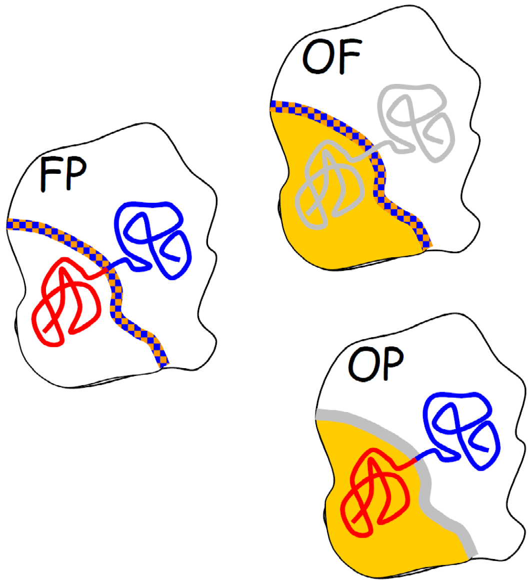

Fig. 5.12: *Scheme of scattering functions for the cross terms within the microemulsion. There are the film-polymer scattering $S_{\rm FP}$, the oil-film scattering $S_{\rm OF}$, and the oil-polymer scattering $S_{\rm OP}$. The real space correlation function means a convolution of two structures.*

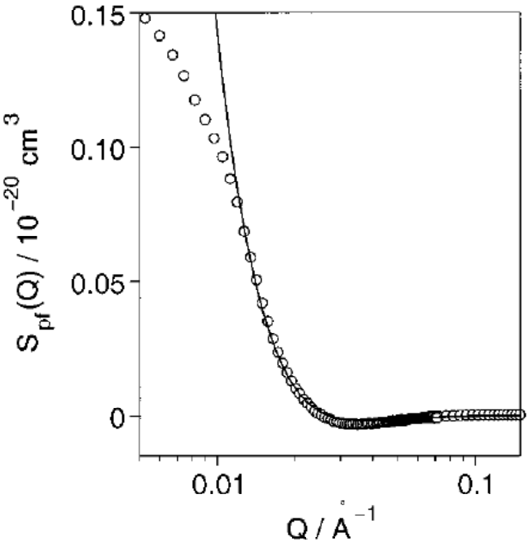

Fig. 5.13: *A measurement of the film-polymer scattering for a bicontinuous microemulsion with a symmetric amphiphilic polymer. The solid line is described by a polymer anchored in the film. The two blocks are mushroom-like in the domains. At low Q the overall domain structure (or size) limits the idealized model picture.*

$$\frac{d\Sigma}{d\Omega}(\mathbf{Q}) = \frac{1}{V}\cdot\sum_{j,k=2}^{n}\Delta\rho^*_{j1}(\mathbf{Q})\cdot\Delta\rho_{k1}(\mathbf{Q}) \tag{5.38}$$

$$= \sum_{j,k=2}^{n}(\Delta\rho_{j1}\Delta\rho_{k1})\cdot S_{jk}(\mathbf{Q}) \tag{5.39}$$

$$= \sum_{j=2}^{n}(\Delta\rho_{j1})^2\cdot S_{jj}(\mathbf{Q}) \;+\; 2\sum_{2<j<k\le n}(\Delta\rho_{j1}\Delta\rho_{k1})\cdot\Re\, S_{jk}(\mathbf{Q}) \tag{5.40}$$

In line 5.39 the scattering function $S_{jk}(\mathbf{Q})$ is defined. By this the contrasts are separated from the Q-dependent scattering functions. Finally, in line 5.40 the diagonal and off-diagonal terms are collected. There are $n-1$ diagonal terms, and $\frac{1}{2}(n-1)(n-2)$ off-diagonal terms. Formally, these $\frac{1}{2}n(n-1)$ considerably different terms are rearranged (the combinations $\{j,k\}$ are now simply numbered by j), and a number of s different measurements with different contrasts are considered.

$$\left.\frac{d\Sigma}{d\Omega}(\mathbf{Q})\right|_s = \sum_j(\Delta\rho\cdot\Delta\rho)_{sj}\cdot S_j(\mathbf{Q}) \tag{5.41}$$

In order to reduce the noise of the result, the number of measurements s exceeds the number of independent scattering functions considerably. The system then becomes over-determined when solving for the scattering functions. Formally one can nonetheless write:

$$S_j(\mathbf{Q}) = \sum_s (\Delta\rho \cdot \Delta\rho)^{-1}_{sj} \cdot \left.\frac{d\Sigma}{d\Omega}(\mathbf{Q})\right|_s \tag{5.42}$$

The formal inverse matrix $(\Delta\rho \cdot \Delta\rho)^{-1}_{sj}$ is obtained by the singular value decomposition method. It describes the closest solution of the experiments in context of the finally determined scattering functions.

An example case is discussed for a bicontinuous microemulsion with an amphiphilic polymer [7]. The microemulsion consists of oil and water domains which have a sponge structure. So the water domains host the oil and vice versa. The surfactant film covers the surface between the oil and water domains. The symmetric amphiphilic polymer position and function was not clear beforehand. From phase diagram measurements it was observed that the polymer increases the efficiency of the surfactant dramatically. Much less surfactant is needed to solubilize equal amounts of oil and water. Fig. 5.12 discusses the meaning of the cross terms of the scattering functions. Especially the film-polymer scattering is highly interesting to reveal the polymer role inside the microemulsion (see Fig. 5.13). By the modeling it was clearly observed that the amphiphilic polymer is anchored in the membrane and the two blocks describe a mushroom inside the oil and water domains. So basically, the polymer is a macro-surfactant. The effect of the polymer on thermodynamics and the microscopic picture is discussed in chapter 5.3.5.

5.3.3 Scattering of a polymer

In this section we derive the scattering of a single (isolated) polymer coil. This model is the basis for many more complicated models of polymers in solution, polymeric micelles, polymer melts, diblock and multiblock copolymers and so on. So the understanding of these concepts is rather important for scattering experiments on any kind of polymer systems.

This example starts apart from many other calculations from point-like monomers (see eq. 5.14). These monomers are found along a random walk with an average step width of ℓ_K. We try to argue for non-ideal chain segments, but finally will arrive at an expression for rather ideal polymers. For the scattering function we obtain (definition of $S(Q)$ in eq. 5.39-5.41):

$$S(\mathbf{Q}) \propto \frac{1}{N}\sum_{j,k=0}^{N} \left\langle \exp\left(\mathrm{i}\mathbf{Q}\cdot(\mathbf{R}_j - \mathbf{R}_k)\right) \right\rangle \tag{5.43}$$

$$\propto \frac{1}{N}\sum_{j,k=0}^{N} \exp\left\langle -\tfrac{1}{2}\left(\mathbf{Q}\cdot(\mathbf{R}_j - \mathbf{R}_k)\right)^2 \right\rangle \tag{5.44}$$

$$\propto \frac{1}{N}\sum_{j,k=0}^{N} \exp\left\langle -\tfrac{1}{6}\mathbf{Q}^2\cdot(\mathbf{R}_j - \mathbf{R}_k)^2 \right\rangle \tag{5.45}$$

At this stage we use statistical arguments (i.e. statistical physics). The first rearrangement of terms (line 5.44) moves the ensemble average of the monomer positions (and distances $\Delta\mathbf{R}_{jk}$) from the outside of the exponential to the inside. This is an elementary step which is true for polymers. The underlying idea is that the distance $\Delta\mathbf{R}_{jk}$ arises from a sum of $|j-k|$ bond vectors which all have the same statistics. So each sub-chain with the indices jk is only distinguished by its number of bond vectors inside. The single bond vector $\mathbf{b}_j$ has a statistical average of $\langle\mathbf{b}_j\rangle = 0$ because there is no preferred orientation. The next higher moment is the second moment $\langle\mathbf{b}_j^2\rangle = \ell_K^2$. This describes that each bond vector does a finite step with an average length of ℓ_K. For the sub-chain we then find an average size $\langle\Delta\mathbf{R}_{jk}^2\rangle = |j-k|\ell_K^2$. The reason is that in the quadrature of the sub-chain only the diagonal terms contribute because two distinct bond vectors show no (or weak) correlations.

Back to the ensemble average: The original exponential can be seen as a Taylor expansion with all powers of the argument $\mathrm{i}\mathbf{Q}\Delta\mathbf{R}_{jk}$. The odd powers do not contribute with similar arguments than for the single bond vector $\langle\mathbf{b}_j\rangle = 0$. Thus, the quadratic term is the leading term. The reason why the higher order terms can be arranged that they finally fit to the exponential expression given in line 5.44 is the weak correlations of two distinct bond vectors. The next line 5.45 basically expresses the orientational average of the sub-chain vector $\Delta\mathbf{R}_{jk}$ with respect to the Q-vector in three dimensions.

This derivation can be even simpler understood on the basis of a Gaussian chain. Then every bond vector follows a Gaussian distribution (with a center of zero bond length). Then the ensemble average has the concrete meaning $\langle\cdots\rangle = \int\cdots\exp\left(-\frac{3}{2}\Delta\mathbf{R}_{jk}^2/(|j-k|\ell_K^2)\right)d^3\Delta R_{jk}$. This distribution immediately explains the rearrangement of line 5.44. The principal argument is the central limit theorem: When embracing several segments as an effective segment any kind of distribution converges to yield a Gaussian distribution. This idea came from Kuhn who formed the term Kuhn segment. While elementary bonds still may have correlations at the stage of the Kuhn segment all correlations are lost, and the chain really behaves ideal. This is the reason why the Kuhn segment length ℓ_K was already used in the above equations.

In the following we now use the average length of sub-chains (be it Kuhn segments or not), and replace the sums by integrals which is a good approximation for long chains with a large number of segments N.

$$S(\mathbf{Q}) \propto \frac{1}{N}\int_0^N dj\int_0^N dk\exp\left(-\tfrac{1}{6}\mathbf{Q}^2\cdot|j-k|\cdot\ell_K^2\right) \tag{5.46}$$

$$= N\cdot f_D(Q^2R_g^2) \tag{5.47}$$

$$f_D(x) = \tfrac{2}{x^2}\left(\exp(-x)-1+x\right) \tag{5.48}$$

In this integral one has to consider the symmetry of the modulus. The result is basically the Debye function which describes the polymer scattering well from length scales of the overall coil down to length scales where the polymer becomes locally rigid (see Fig. 5.14). The covalent bonds of a carbon chain effectively contribute to a certain rigidity which will not be treated here. The radius of gyration describes the overall dimension of the chain and is $R_g = \sqrt{N/6}\,\ell_K$. The limits of the polymer scattering are found to be:

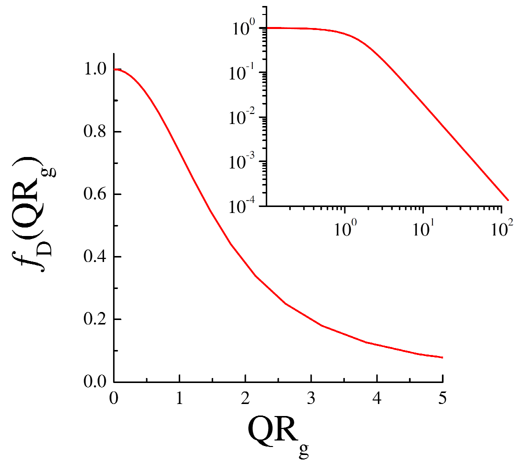

Fig. 5.14: *The theoretical Debye function describes the polymer scattering of independent polymers without interaction. The two plots show the function on a linear and double logarithmic scale.*

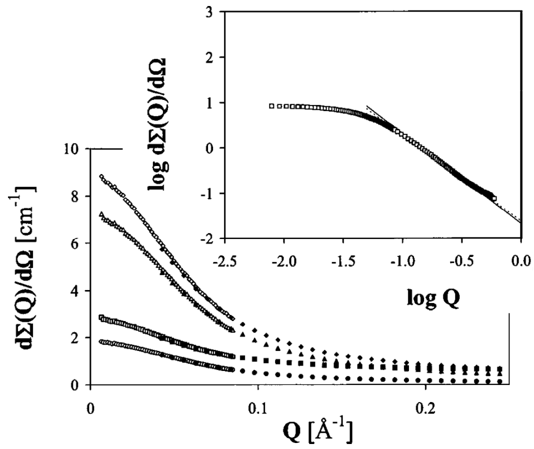

Fig. 5.15: *Scattering of a h/d-PDMS polymer blend. The linear scale shows different compositions of hydrogenous polymer (from bottom to top: 0.05, 0.94, 0.27, 0.65) while the double logarithmic plot shows the 0.65 sample only [8].*

$$S(\mathbf{Q}) \propto N(1 - \tfrac{1}{3}Q^2R_g^2) \qquad \text{for small } Q \tag{5.49}$$

$$\propto N \cdot 2/(Q^2R_g^2) \qquad \text{for large } Q \tag{5.50}$$

The line 5.49 describes the conventional Guinier scattering of the overall polymer (compare eq. 5.35). The second line 5.50 describes a power law. At these length scales the sub-chains of different lengths are self-similar and so they reveal a fractal behavior. The prefactor is connected to the magnitude R_g^2/N which is the effective segment size. From this magnitude one can calculate back to the local rigidity which is responsible for the effective segments.

When we want to compare experiments with this theory the best examples are obtained from polymer blends (Fig. 5.15). One could come to the conclusion that diluted polymer solutions must provide the ideal conditions for such an experiment but practically the interactions of the solvent molecules with the monomers lead to a deviating behavior: The good solvent conditions lead to energetic violations of monomer-monomer contacts and so the polymer swells and displays a different fractal behavior. The high Q power law in good solvents comes close to $Q^{-1.7}$. The Flory theory was the first attempt to describe this behavior while many refinements find small corrections. The theoretically most precise Flory exponent is $\nu = 0.588$ which is the reciprocal value of the given exponent 1.7 above.

So polymer blends are often better examples for weakly interacting chains. This finding is supported by the low entropy of mixing which enforces small interactions. The discussed example of Fig. 5.15 [8] considers the isotopic mixture of hydrogenous and deuterated polydimethylsiloxane (PDMS). This practically leads to one of the lowest possible interactions even though they are not completely zero. The theoretical concept of the random phase approximation is able to deal with interactions and describes phase diagrams and the scattering in this way. At

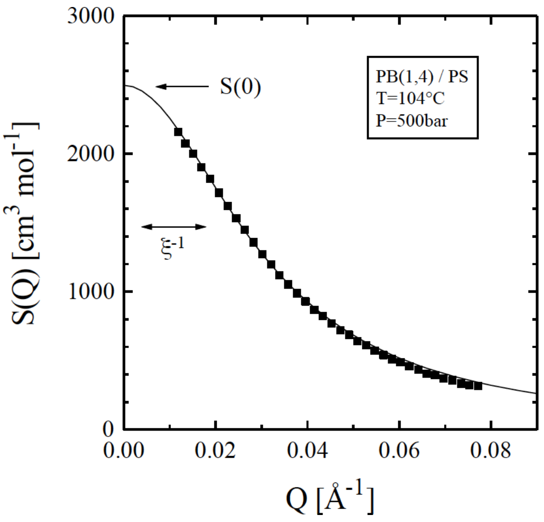

Fig. 5.16: *Typical scattering of a homopolymer blend with interactions. The sample is a polybutadiene(1,4) / polystyrene blend at 104°C and 500bar [9].*

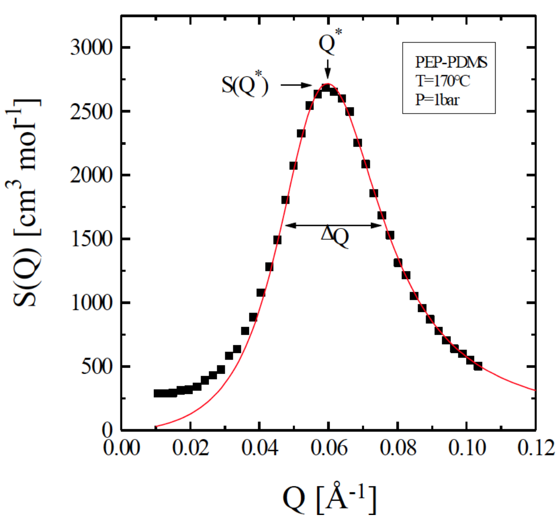

Fig. 5.17: *Typical scattering of a diblock copolymer blend with interactions [10]. The poly-ethylene-propylene–poly-dymethylsiloxane is heated to 170°C (1bar).*

high temperatures the polymers usually mix well, and the scattering comes closer to the weakly interacting case. Closer to the demixing temperature at lower temperatures the scattering intensity increases dramatically. This indicates strong composition fluctuations. The system loses the tendency to form a homogenous mixture and so local enrichments of species A or B are possible. While the random phase approximation is a mean field concept which describes weak fluctuations there are other concepts for strong fluctuations close to the phase boundary: The 3-dimensional Ising model – known for ferromagnets – describes the strong fluctuations of the two component polymer system.

The example of an interacting homopolymer blend is shown in Fig. 5.16. The general aspects are kept from non-interacting polymers (compare Fig. 5.15). The scattering curve has a maximum at $Q = 0$, and is decaying to large Q where a power law of Q^{-2} for ideal chains is observed. The maximal intensity is connected to the reciprocal susceptibility which describes the tendency of spontaneous thermal fluctuations to decay. High intensities mean low susceptibilies and strong fluctuations – the vice versa arguments are valid. The width of this curve is connected to the correlation length ξ. At low interactions it is tightly connected to the single coil size, i.e. R_g. With strong fluctuations close to the phase boundary the correlation length tends to diverge, which measures the typical sizes of the thermally fluctuating enrichments.

A diblock copolymer is a linear chain with two different monomer species. The first part is pure A and the latter pure B. The typical scattering of a diblock copolymer blend is shown in Fig. 5.17. At small Q the ideal scattering increases with Q^2 accordingly to the ‘correlation hole’. The chemistry of the molecule does not allow for enrichments of A or B on large length scales. A continuously growing volume would only allow for enrichments on the surface – this explains finally the exponent in the scattering law. The experimental finite intensities relate to imperfections of the molecules. The chain length ratio f is distributed, and finally allows for enrichments on large length scales.

The dominating fluctuations are found at a finite Q^*. This expresses that the coil allows for separations of A and B predominantly on the length scale of the overall coil. Close to the phase boundary and especially below (where the polymer undergoes a micro phase separation) the coils are stretched. The peak at finite Q^* also expresses that the fluctuations tend to form alternating enrichments. From a center it would look like a decaying order of A-B-A-B-... The width of the peak is again connected to the correlation length $\xi \sim \Delta Q^{-1}$ which describes the length of this decaying order. At high Q, again a Q^{-2} law is observed describing the sub-chains being ideal chains. On these length scales homopolymer blends and diblock copolymers do not differ.

The whole understanding of phase boundaries and fluctuations is important for applications. Many daily life plastic products consist of polymer blends since the final product should have combined properties of two different polymers. Therefore, polymer granulates are mixed at high temperatures under shear in an extruder. The final shape is given by a metal form where the polymer also cools down. This process involves a certain temperature history which covers the one-phase and two-phase regions. Therefore, the final product consists of many domains with almost pure polymers. The domain size and shape are very important for the final product. So the process has to be tailored in the right way to yield the specified domain structure. This tailoring is supported by a detailed knowledge of the phase boundaries and fluctuation behavior. Advanced polymer products also combine homopolymers and diblock copolymers for an even more precise and reproducible domain size/shape tailoring [11, 12]. The diblock copolymer is mainly placed at the domain interfaces, and, therefore, influences the domain properties precisely.

5.3.4 The structure factor

In this section we develop the ideas about the structure factor – an additional factor for the scattering formula (eq. 5.32) – which describes the effect of interactions between the colloids or particles. We start from a rather simple interaction for colloids. It simply takes into account that the particles cannot intersect. This interaction is called excluded volume interaction. Then the general case will be discussed briefly and conceptually.

We start from the scattering length density for two spheres with different origins $\mathbf{R}_1$ and $\mathbf{R}_2$. In this case the formula reads:

$$\Delta\rho(\mathbf{Q}) = \Delta\rho \cdot V_{\text{sphere}} \cdot \big(\exp(\mathrm{i}\mathbf{Q}\mathbf{R}_1) + \exp(\mathrm{i}\mathbf{Q}\mathbf{R}_2)\big) \cdot K(Q,R) \qquad (5.51)$$

$$K(Q,R) = 3 \cdot \frac{\sin(QR) - QR\cos(QR)}{(QR)^3} \qquad (5.52)$$

The main difference arises from the phases of the two origins of the two colloids. Otherwise the result is known from eq. 5.31. For the macroscopic cross section we rearrange the amplitudes in the following way:

$$\frac{d\Sigma}{d\Omega}(\mathbf{Q}) = (\Delta\rho)^2 \cdot \frac{2V_{\text{sphere}}}{V_{\text{tot}}} \cdot V_{\text{sphere}} \cdot \left|\exp(\mathrm{i}\mathbf{Q}\mathbf{R}_1)\right|^2 \cdot \left\langle \frac{1}{2}\left|1+\exp(\mathrm{i}\mathbf{Q}\Delta\mathbf{R})\right|^2 \right\rangle_{\Delta\mathbf{R}} \cdot K^2(Q,R) \tag{5.53}$$

There are factors for the contrast, the concentration, the single particle volume, one phase factor which results in 1, one factor for the relative phases, and the form factor. In comparison to eq. 5.32 all factors are known except for the factor about the relative phases. The brackets describe an ensemble average known from statistical physics. We have to consider all possible relative positions $\Delta\mathbf{R}$. This is done in the following:

$$S(Q) = \left\langle \frac{1}{2}\left|1+\exp(\mathrm{i}\mathbf{Q}\Delta\mathbf{R})\right|^2 \right\rangle_{\Delta\mathbf{R}} = \left\langle 1+\cos(\mathbf{Q}\Delta\mathbf{R})\right\rangle_{\Delta\mathbf{R}} \tag{5.54}$$

$$= \frac{1}{V_{\text{tot}}}\left(V_{\text{tot}} + 2\pi\delta(\mathbf{Q}) - \frac{4\pi}{3}(2R)^3 K(Q,2R)\right) \tag{5.55}$$

The main result is found in line 5.55 which is obtained from the ensemble average. The prefactor arises from the normalization. The constant term arises from integrating over the whole volume. To be more precise the vector $\mathbf{R}$ has to omit a volume of a sphere with the radius $2R$, because this is the minimum distance of the two centers. For the integral of the constant contribution we neglect this small difference. For the integral over the cosine function we have to do a trick which is called the Babinet principle: The really allowed volume is the sum of the full volume minus the sphere with the radius $2R$. The cosine function integrated over the full volume is again a delta function, and the subtracted term is the Fourier transformation of a sphere, i.e. $K(Q,2R)$. We obtain the same result for the cosine-Fourier transformation and the complex Fourier transformation because the volume is centro-symmetric. The Babinet principle actually uses the inversion of the volume and states for squares of amplitudes, i.e. intensities, exactly the same result as for the original structure. For the structure factor we have to keep in mind: It arises from a single Fourier transformation and is not squared. The final result in brief is (neglecting the delta function again):

$$S(\mathbf{Q}) = 1 - \phi_{2R} \cdot K(Q,2R) \tag{5.56}$$

$$\frac{d\Sigma}{d\Omega}(\mathbf{Q}) = (\Delta\rho)^2 \cdot \phi_{\text{sphere}} \cdot V_{\text{sphere}} \cdot S(\mathbf{Q}) \cdot K^2(Q,R) \tag{5.57}$$

So we obtain the well known factors for the macroscopic cross section – now with a structure factor. The form and structure factor are compared in Fig. 5.18. The reduced intensity at small scattering vectors due to the structure factor appears for repulsive interactions and means that the possible fluctuations of the particles are reduced because they have less freedom. The first maximum indicates a preferred distance between the colloids. Such a maximum becomes more pronounced with higher concentrations. Note that for this example the maximum appears at a Q where the form factor already has a downturn. There are many examples in the literature where the form factor is still relatively close to 1 and then the structure factor is exposed very clearly.

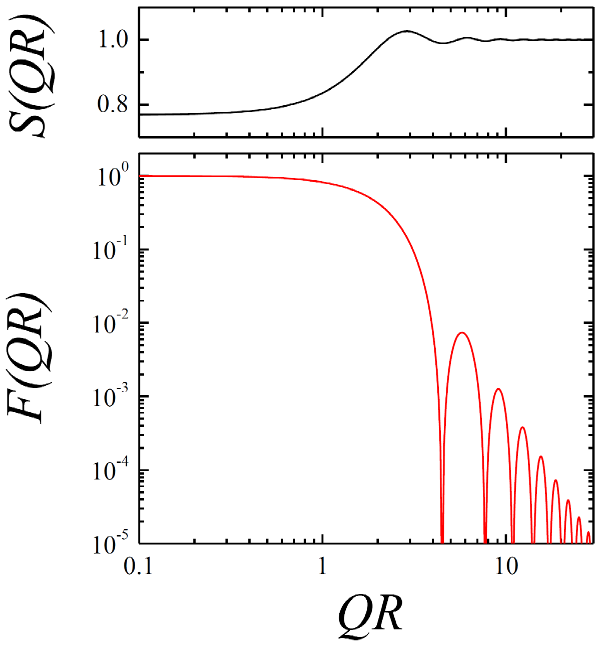

Fig. 5.18: *The structure factor $S(Q)$ on top of the form factor $F(Q) = K^2(Q)$. Note that the structure factor is smaller than 1 for small Q. This indicates a repulsive interaction. The first maximum of the structure factor expresses a certain tendency for preferred distances. Of course it only appears for rather strong concentrations.*

So far we have derived the excluded volume structure factor for very dilute systems. The method of Ornstein-Zernicke allows for a simple refinement by describing higher order correlations on the basis of the simple pair correlation. Then – in the simplest way – one would obtain the following expression:

$$S_2(\mathbf{Q}) = \big(1 + \phi_{2R} \cdot K(Q, 2R)\big)^{-1} \tag{5.58}$$

A more rigorous treatment of the Ornstein-Zernicke formalism results in the Perkus-Yevick structure factor [13] which is the best known approximation for hard spheres. On the basis of this structure factor as the dominating term small corrections for additional interactions can be included [14]. For colloidal systems this is the strategy of choice.

Nonetheless, we would like to understand the structure factor more generally. From equation 5.54 we have seen that the phases of two centers have to be considered. The ensemble average finally took the distribution of possible distance vectors $\Delta\mathbf{R}$ into account. So we can understand the structure factor on the basis of a pair correlation function for the centers of the particles.

$$S(\mathbf{Q}) = 1 + \phi \int_V d^3r \, \big(g(\mathbf{r}) - 1\big) \exp(\mathrm{i}\mathbf{Q}\mathbf{r}) \tag{5.59}$$

The function $g(\mathbf{r})$ is the pair correlation function and describes the probabilities for certain distance vectors $\mathbf{r}$, and the exponential function accounts for the phases. Again, for centro-symmetric $g(\mathbf{r})$ there is no difference between a cosine and a complex Fourier transformation. The subtraction of the constant 1 accounts for delta peak contributions which we also obtained

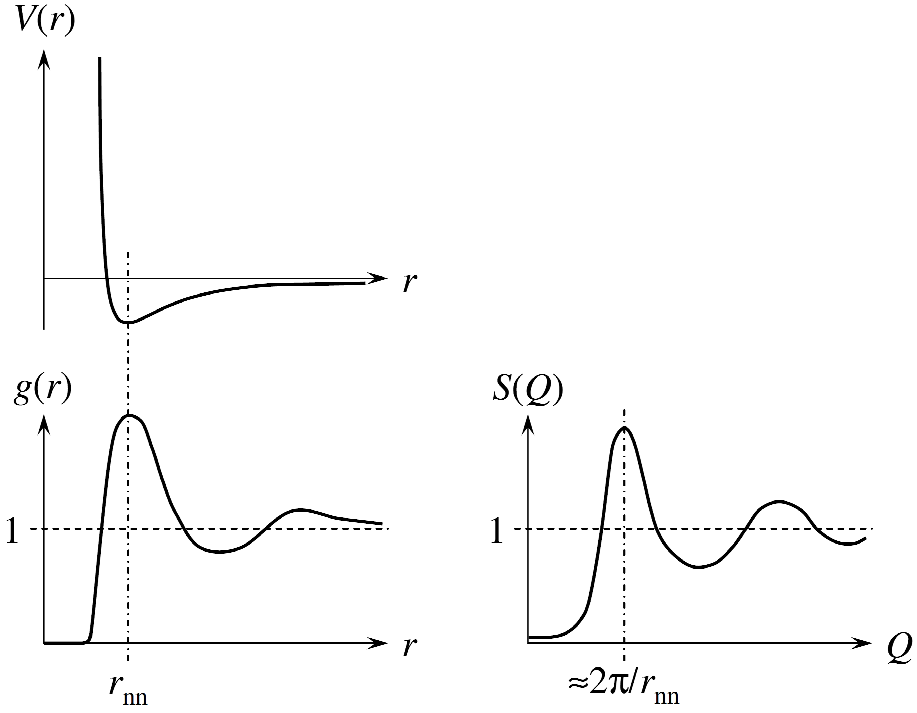

Fig. 5.19: *The relation between the interaction potential $V(r)$, the pair correlation function $g(r)$ in real space, and the structure factor $S(Q)$.*

in line 5.55. The added term 1 we also obtained in the beginning (line 5.54). It arises from the self correlation of the particle with itself. For the pair distribution function we now can write:

$$g(\mathbf{r}_2 - \mathbf{r}_1) = \frac{P(\mathbf{r}_1, \mathbf{r}_2)}{P(\mathbf{r}_1) \cdot P(\mathbf{r}_2)}, \qquad \text{and} \;\; \phi = P(\mathbf{r}_1) \tag{5.60}$$

and can be obtained theoretically with methods from statistical physics. It describes the probability for finding two particles at a distance $\mathbf{r}_2 - \mathbf{r}_1$. A rather elementary example is discussed in Fig. 5.19 starting from an interaction potential $V(\mathbf{r})$. It has a repulsive short range interaction, a weak minimum at a distance r_{nn}, and a quickly decaying tail to long distances. The distance r_{nn} indicates the preferred distance of nearest neighbors. The pair correlation function then shows an inhibited range at short distances – similar to an excluded volume interaction. The following peak at r_{nn} indicates a preferred nearest neighbor distance. The following oscillations for larger distances indicate more remote preferred places. The limit of $g(\mathbf{r})$ at large distances is 1 indicating the average concentration of particles. For the structure factor we obtain a rather strong suppression at small Q. This means that the repulsive interactions lead effectively to a more homogenous distribution of particles. The peak of the structure factor at $Q = 2\pi/r_{\mathrm{nn}}$ indicates the preferred distance of the nearest neighbors. Strong oscillations at higher Q indicate a narrow distribution of the actual neighbor distances. The limit at high Q is again 1, and arises from the self correlation of identical particles. This example describes a liquid-like behavior which has historically been developed for liquids. In soft matter research this concept applies for many systems ranging from colloids, over micelles to star-polymers. While the liquid-like structure describes a near order, a perfect crystal would lead to a different behavior: The correlation function $g(\mathbf{r})$ would contain a lattice of separated delta peaks. The structure factor would describe the reciprocal lattice with the well known Bragg peaks. In soft matter research there exist many examples with liquid crystalline order. Very often they display a finite size of crystalline domains – so there is a grain structure – and the real state takes an intermediate stage between the perfect crystalline and liquid-like order.

5.3.5 Microemulsions

In this section we will follow a very successful way of deriving the scattering formula for bicontinuous microemulsions (see Fig. 5.20). Bicontinuous microemulsions consist of equal amounts of oil and water. A certain amount of surfactant is needed to solubilize all components, and a one phase system is obtained. The domain structure of the oil is a continuous sponge structure which hosts the water and vice versa. The surfactant forms a film at the surface between the oil and water domains.

The starting point is a thermodynamic model for such kind of system. The Landau approach takes mesoscopic sub-volumes and assumes that the internal degrees of freedom are integrated out, and there is a small number of order parameters describing the state of the sub-volume very accurately. For microemulsions we stay with a single (scalar) order parameter $\phi(\mathbf{r})$ which takes the values -1 for oil, 0 for surfactant, and $+1$ for water. Now the order parameter can still be treated like a continuous function since the physical effects take place on larger length scales than the sub-volume size. The (free) energy of the overall volume is now expressed as a function of the order parameter. One still cannot be perfectly accurat, so an expansion with respect to the order parameter is used. The expansion for microemulsions looks like:

$$F_0\big(\phi(\mathbf{r})\big) = \int d^3r \big[c(\nabla^2\phi)^2 + g_0(\nabla\phi)^2 + \omega_2\phi^2\big] \tag{5.61}$$

This expansion does not only contain the order parameter itself, but there are derivatives included. These appear since this expression of the free energy is a functional expansion. Certain orders (especially the odd orders) of the order parameter and its derivatives have been ruled out due to the symmetry of the system. One important symmetry is the restriction to equal amounts of oil and water. Another facilitating property is that the functional form only considers local contributions in the functional form. For this free energy expression one can apply statistical physics methods and derive a scattering function (done in Appendix C). In comparison with the real space correlation function one can identify two important parameters: the correlation length ξ and the wavevector of the domain spacing $k = 2\pi/d$. The obtained scattering function looks like:

$$\left.\frac{d\Sigma}{d\Omega}(\mathbf{Q})\right|_{\mathrm{TS}} = (\Delta\rho_{\text{oil–water}})^2 \frac{8\pi\phi_{\text{oil}}\phi_{\text{water}}/\xi}{(k^2+\xi^{-2})^2 - 2(k^2-\xi^{-2})\mathbf{Q}^2 + \mathbf{Q}^4} \tag{5.62}$$

This function is also known as the Teubner-Strey formula [15]. While the applied concept approaches the reality as a long wavelength description, there are details missing. The described domains have rather plain walls while in reality the domain walls also fluctuate quite heavily. An empirical approach for the scattering function for the full Q-range is the following:

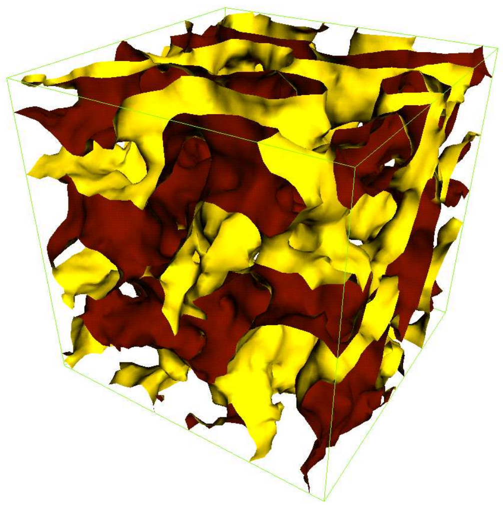

Fig. 5.20: *A real space picture of the bicontinuous microemulsion according to computer simulations [16]. Actually the surfactant film is shown with the surface color being red for oil facing surface and yellow for water facing surface.*

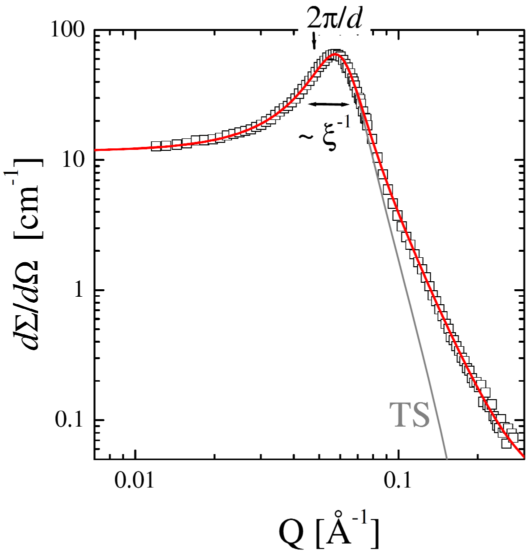

Fig. 5.21: *The macroscopic cross section of a bicontinuous microemulsion. The peak indicates an alternating domain structure with the spacing d. The peak width is connected to the correlation length ξ. The grey line is the simple Teubner-Strey fitting while the red line corresponds to eq. 5.63.*

$$\frac{d\Sigma}{d\Omega}(\mathbf{Q}) = \left[\frac{d\Sigma}{d\Omega}(\mathbf{Q})\bigg|_{\mathrm{TS}} + \frac{G\ \mathrm{erf}^{12}(1.06 \cdot QR_g/\sqrt{6})}{1.5 \cdot Q^4 R_g^4} \right] \cdot \exp\left(-\sigma^2 Q^2\right) \tag{5.63}$$

The error function $\mathrm{erf}(x)$ in the overall context describes a peak with a Porod behavior at large Q. This additional Porod term accounts for the larger surface of the fluctuating membranes. The final Gaussian factor describes a roughness of the surfactant film and often is not that clearly observed due to the high incoherent background. An example fit of this function to scattering data is discussed in Fig. 5.21. The pure Teubner-Strey function clearly shows a downturn at higher Q and the real Porod scattering is not well described. Only the additional Porod scattering allows for a realistic estimation of the averge surface of the domain structure.

From the structural parameters $k = 2\pi/d$ and ξ one can make connections to the microscopic parameters of the microemulsion. The Gaussian random field theory describes the thermodynamics of a microemulsion by using a wave field that places the surfactant film at the zero surfaces of the field. The theory makes a connection of the structural parameters to the bending rigidity:

$$\frac{\kappa}{k_B T} = \frac{5\sqrt{3}}{64} \cdot k\xi \tag{5.64}$$

The bending rigidity κ is an elastic modulus of the surfactant membrane. The overall underlying concept only relies on the elastic properties of the membrane to describe the thermodynamics

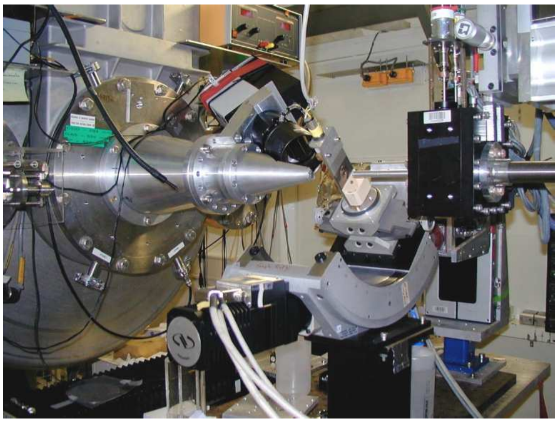

Fig. 5.22: *The sample position of the SAXS instrument ID2 at the ESRF, Grenoble, France. The photons propagate from the right to the left. The collimation guides on the left and the detector tank window on top of the cone on the left give an impression about the small beam size (being typically 1×1mm^2).*

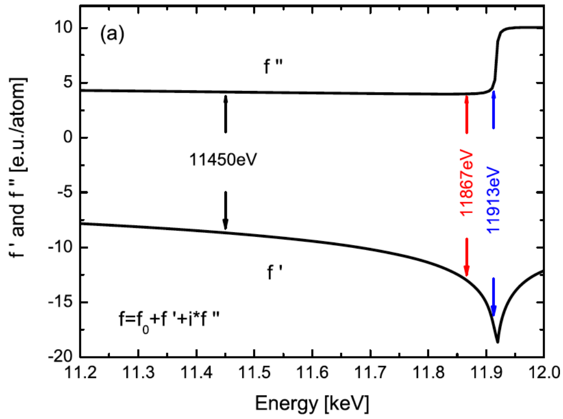

Fig. 5.23: *The complex dispersion curve for gold (Au) at the L_3 edge [17]. The overall effective electron number $f = f_0 + f' + \mathrm{i}f''$ replaces the conventional electron number $Z = f_0$ in equation 5.65. On the x-axis the energies of the x-rays is shown, with indications for the experimentally selected three energies (black, red, blue). In this way, equal steps for the contrast variation are achieved.*

of bicontinuous microemulsions. For symmetric amphiphilic polymers it was found that the bending rigidity increases [7]. The reason is that the mushroom conformation (obtained by the contrast variation measurements from chapter 5.3.2) exerts a pressure on the membrane. This makes the membrane stiffer which in turn allows to form larger domains with a better surface to volume ratio. So the much lower demand for surfactant is explained on the basis of small angle neutron scattering experiments.

5.4 Small angle x-ray scattering

While a detailed comparison between SANS and SAXS is given below, the most important properties of the small angle x-ray scattering technique shall be discussed here. The x-ray sources can be x-ray tubes (invented by Röntgen, keyword Bremsstrahlung) and modern synchrotrons. The latter ones guide fast electrons on undulators which act as laser-like sources for x-rays with fixed wavelength, high brilliance and low divergence. This simply means that the collimation of the beam often yields narrow beams, and the irradiated sample areas are considerably smaller (often smaller than ca. 1×1mm^2). A view on the sample position is given in Fig. 5.22 (compare Fig. 5.3). One directly has the impression that all windows are tiny and adjustments must be made more carefully.

The conceptual understanding of the scattering theory still holds for SAXS. For the simplest understanding of the contrast conditions in a SAXS experiment, it is sufficient to count the electron numbers for each atom. The resulting scattering length density reads then (compare eq. 5.16):

$$\rho_{\mathrm{mol}} = \frac{r_e}{V_{\mathrm{mol}}} \sum_{j \in \{\mathrm{mol}\}} Z_j \tag{5.65}$$

The classical electron radius is $r_e = \mathrm{e}^2/(4\pi\epsilon_0 m_e c^2) = 2.82\mathrm{fm}$. The electron number of each atom j is Z_j. This means that chemically different substances have a contrast, but for similar substances (often for organic materials) it can be rather weak. Heavier atoms against light materials are much easier to detect. Finally, the density of similar materials is also important. Especially for organic materials (soft matter research), the high intensity of the source still allows for collecting scattering data. Many experiments base on these simple modifications with respect to SANS, and so the fundamental understanding of SAXS experiments does not need any further explanation.

For completeness, we briefly discuss the scattering length density for light scattering. Here the polarizability plays an important role. Without going into details, the final contrast is expressed by the refractive index increment dn/dc:

$$\rho_{\mathrm{mol}} = \frac{2\pi n}{\lambda^2} \cdot \frac{dn}{dc_{\mathrm{mol}}} \tag{5.66}$$

The refractive index increment dn/dc finally has to be determined separately experimentally when the absolute intensity is of interest. The concentration c_{mol} is given in units volume per volume (for the specific substance in the solvent). The wavelength of the used light is λ.

5.4.1 Contrast variation using anomalous small angle x-ray scattering

While for contrast variation SANS experiments the simple exchange of hydrogen ^{1}H by deuterium ^{2}H $\equiv$ D allowed for changing the contrast without modifying the chemical behavior, in contrast variation SAXS experiments the applied trick is considerably different: The chemistry is mainly dominated by the electron or proton number Z and isotope exchange would not make any difference. The electron shells on the other hand have resonances with considerable dispersion curves. An example is shown in Fig. 5.23 with the real part f' (called dispersion) and the imaginary part f'' (called absorption). The overall effective electron number $f = f_0 + f' + \mathrm{i}f''$ replaces the conventional electron number $Z = f_0$ in equation 5.65. Below the resonance energy the considered L_3 shell appears only softer and effectively less electrons appear for f. Above the resonance energy single electrons can be scattered out from the host atom (Compton effect). This is directly seen in the sudden change of the absorption. Furthermore, the actual dependence of the dispersion is influenced by backscattering of the free electrons to the host atom (not shown in Fig. 5.65). This effect finally is the reason that the complex dispersion curve can only theoretically be well approximated below the resonance (or really far above). For this approximation it is sufficient to consider isolated host atoms.

For best experimental results the f-values have to be equally distributed. Thus, the energies are selected narrower close to the resonance (see Fig. 5.65). The investigated sample consisted of core-shell gold-silver nanoparticles in soda-lime silicate glass (details in reference [17]). By the contrast variation measurement one wanted to see the whole particles in the glass matrix, but also the core-shell structure of the individual particles. Especially, the latter one would be obtained from such an experiment. First results of this experiment are shown in Fig. 5.24. The most important result from this experiment is that the original scattering curves at first hand do not differ considerably. The core-shell structure results from tiny differences of the measurements. For contrast variation SANS experiments the contrasts can be selected close to zero contrast for most of the components which means that tiniest amounts of additives can be highlighted and the intensities between different contrasts may vary by factors of 100 to 1000. So for contrast variation SAXS measurements the statistics have to be considerably better which in turn comes with the higher intensities.

Another example was evaluated to a deeper stage [18]. Here, the polyelectrolyte polyacrylate (PA) with Sr^{2+} counterions was dissolved in water. The idea behind was that the polymer is dissolved well in the solvent. The charges of the polymer and the ions lead to a certain swelling of the coil (exact fractal dimensions ν not discussed here). The counterions form a certain cloud around the chain – the structure of which is the final aim of the investigation. The principles of contrast variation measurements leads to the following equation (compare eq. 5.41):

$$\frac{d\Sigma}{d\Omega} = (\Delta\rho_{\mathrm{Sr-H2O}})^2 \cdot S_{\mathrm{Sr-Sr}} + (\Delta\rho_{\mathrm{PA-H2O}})^2 \cdot S_{\mathrm{PA-PA}} + \Delta\rho_{\mathrm{Sr-H2O}}\Delta\rho_{\mathrm{PA-H2O}} \cdot S_{\mathrm{Sr-PA}} \quad (5.67)$$

The overall scattering is compared with two contributions in Fig. 5.25. The scattering functions of the cross term $S_{\mathrm{Sr-PA}}$ and the pure ion scattering $S_{\mathrm{Sr-Sr}}$ have been compared on the same scale, and so the contrasts are included in Fig. 5.25. Basically, all three functions describe a polymer coil in solvent – the different contrasts do not show fundamental differences. Nonetheless, a particular feature of the ion scattering was highlighted by this experiment: At $Q \approx 0.11\mathrm{nm}^{-1}$ is a small maximum which is connected to the interpretation of effective charge beads along the chains. The charge clouds obviously can be divided into separated beads. The emphasis of the observed maximum correlates with the number of beads: For small numbers it is invisible, and becomes more pronounced with higher numbers. The authors finally find that the number of 5 beads is suitable for the description of the scattering curves: An upper limit is also given by the high Q scattering where the 5 chain segments appear as independent subcoils. This example beautifully displays that the method of contrast variation can be transferred to SAXS experiments. Difficulties of small contrast changes have been overcome by the good statistics due to much higher intensities.

5.4.2 Comparison of SANS and SAXS

We have seen that many parallels exist between the two experimental methods SANS and SAXS. The theoretical concepts are the same. Even the contrast variation method as a highly difficult and tedious task could be applied for both probes. In the following, we will highlight differences that have been discussed so far, and others that are just mentioned now.

The high flux reactors are at the technical limit of highest neutron fluxes. For SANS instruments maximal fluxes of ca. 2×10^8 neutrons/s/cm^2 have been reached at the sample position. Typical sample sizes are of $1\times1\mathrm{cm}^2$. For coherent scattering fractions of ca. 10% this results in maximal count rates of 10^7Hz, while practically most of the count rates stay below 10^6Hz. For long collimations, the experimentalists deal often with 10 to 50Hz. The resolution for these count

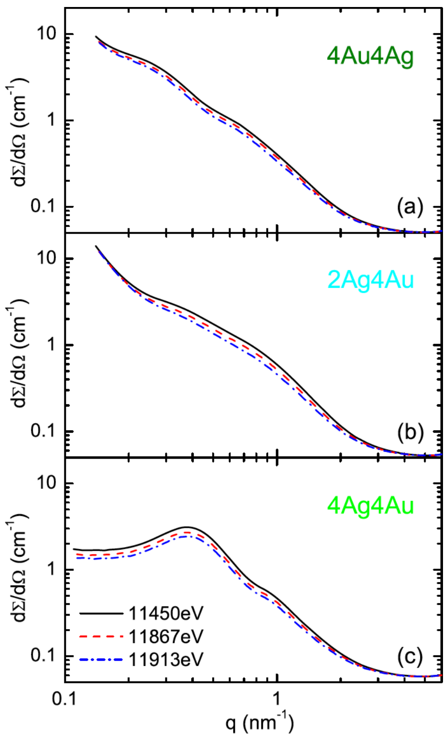

Fig. 5.24: *Absolute calibrated scattering curves of different core-shell Ag/Au nanoparticles in soda-lime silicate glass [17]. The implantation sequence has been changed for the three samples. Note that the three scattering curves for the selected energies (colors correspond to Fig. 5.23) do only slightly differ due to the small changes of the contrast.*

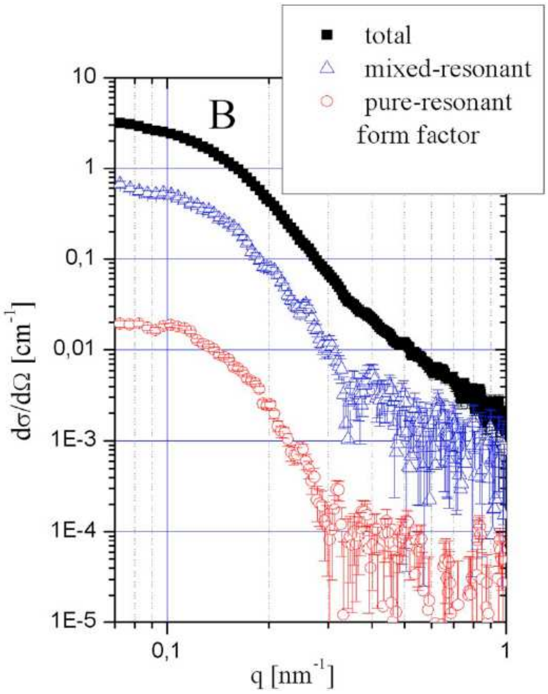

Fig. 5.25: *Further evaluated scattering functions of a different system [18]: A polyelectrolyte with Sr^{2+} counterions in aqueous solution. The top curve (black) indicates the overall scattering. The middle curve (blue) displays the polymer-ion cross terms being sensitive for relative positions. The bottom curve (red) depicts the pure ion scattering.*

rates has been relaxed. Wavelength spreads of either ±5% or ±10% are widely accepted, and the collimation contributes equally, such that a typical resolution of $\Delta Q/Q$ of 7 to 14% is reached. For many soft matter applications this is more than adequate. If one thinks of liquid crystalline order, much higher resolution would be desired which one would like to overcome by choppers in combination with time-of-flight analysis. A resolution of ca. 1% would be a reasonable expectation. The continuous sources are highly stable which is desired for a reliable absolute calibration.

The spallation sources deliver either continuous beams or the most advanced ones aim at pulsed beams. Repetition rates range from ca. 14 to 60Hz. The intensity that is usable for SANS instruments could reach up to 20 times higher yields (as planned for the ESS in Lund), i.e. up to 4×10^9 neutrons/s/cm^2. Surely, detectors for count rates of 10 to 100 MHz have to be developed. The new SANS instruments will make use of the time-of-flight technique for resolving the different wavelengths to a high degree. Of course other problems with such a broad wavelength band have to be overcome – but this topic would lead too far.

The synchrotron sources reach much higher photon yields which often makes the experiments technically comfortable but for the scientist at work highly stressful. The undulators provide laser-like qualities of the radiation which explains many favorable properties. Some numbers for the SAXS beam line ID2 at the ESRF shall be reported. The usable flux of 5×10^{15} photons/s/mm^2 (note the smaller area) is provided which results for a typical sample area of ca. 1×0.02mm^2 in 10^{14} photons/s. In some respect the smallness of the beam urges to think about the representativeness of a single shot experiment. At some synchrotron sources the beam is not highly stable which makes absolute calibration and background subtraction difficult. The same problem also occurs for the pulsed neutron sources where parts of the calibration procedure become highly difficult.

For classical SANS experiments one can make some statements: The absolute calibration is practically done for all experiments and does not take much effort – it is technically simple. Between different instruments in the world the discrepancies of different calibrations results often in errors of 10% and less. Part of the differences are different calibration standards, but also different concepts for transmission measurements and many details of the technical realization. The nuclear scattering is a result of the fm small nuclei and results in easily interpretable scattering data for even large angles – for point-like scatterers no corrections have to be made. In this way all soft matter and biological researchers avoid difficult corrections. Magnetic structures can be explored by neutrons due to its magnetic moment. Magnetic scattering is about to be implemented to a few SANS instruments. Ideally, four channels are experimentally measured (I_{++}, I_{+-},I_{-+}, and I_{--}) by varying the polarization of the incident beam (up/down) and of the analyzer. Nowadays, the ^{3}He technique allows for covering relatively large exit angles at high polarization efficiencies. But also early magnetic studies have been possible with simpler setups and reduced information. The unsystematic dependence of the scattering length often opens good conditions for a reasonable contrast for many experiments. If the natural isotopes do not provide enough contrast pure isotopes might overcome the problem. The contrast variation experiments have been presented for the SANS technique. By a simple exchange of hydrogen by deuterium, soft matter samples can be prepared for complicated contrast variation experiments. One advantage is the accessibility of the zero contrast for most of the components which allows for highlighting smallest amounts of additives. The high demand for deuterated chemicals makes them cheap caused by the huge number of NMR scientists. The low absorption of neutrons for many materials allows for studying reasonably thick samples (1 to 5mm and beyond). Especially, for contrast variation experiments often larger optical path lengths are preferred. The choice for window materials and sample containers is simple in many cases. Neutron scattering is a non-destructive method. Espeically biological samples can be recovered.

Contrarily we observe for the SAXS technique: The demand for absolute calibration in SAXS experiments is growing. Initial technical problems are overcome and suitable calibration standards have been found. The interpretation of scattering data at larger angles might be more complicated due to the structure of the electron shells. For small angle scattering the possible corrections are often negligible. Magnetic structures are observable by the circular magnetic dichroism [19] but do not count to the standard problems addressed by SAXS. The high contrast of heavy atoms often makes light atoms invisible. For soft matter samples the balanced use of light atoms results in low contrast but, technically, the brilliant sources overcome any intensity problem. The ASAXS technique is done close to resonances of single electron shells and opens the opportunity for contrast variation measurements. The achieved small differences in the contrast still allow for tedious measurements because the statistics are often extremely good – only stable experimental conditions have to be provided. The absorption of x-rays makes the choice of sample containers and windows more complicated. The absorbed radiation destroys the sample in principle. Short experimental times are thus favorable.

To summarize, the method of small angle neutron scattering is good-natured and allows to tackle many difficult tasks. The small angle x-ray scattering technique is more often applied due to the availability. Many problems have been solved (or will be solved) and will turn to standard techniques. So, in many cases the competition between the methods is kept high for the future. Today, practically, the methods are complementary and support each other for the complete structural analysis.

5.5 Summary

We have seen that small angle neutron scattering is a powerful tool to characterize nanostructures. Examples included colloidal dispersions and microemulsions. The structural parameters are connected to thermodynamics and therefore the behavior is understood microscopically.

In many cases, small angle x-ray scattering can obtain the same results. Nonetheless, x-ray samples need to be thinner due to the low transmission, amd radiation damage has to be taken into account. The powerful method of contrast variation is restricted to heavier atoms, and is, therefore, barely used in soft matter research.

Transmission electron microscopy (TEM) measures the structures in real space, and is as such much easier to understand. Nowadays microscopes provide a spatial resolution of nanometers and better. Nonetheless, usually surfaces or thin layers are characterized and the volume properties need to be extrapolated. For statistics about polydispersity single particles need to be counted while the scattering experiment averages over macroscopic volumes. The sample preparation for TEM does not always produce reliable conditions and results.

The beauty of small angle neutron scattering has convinced in many applications ranging from basic research to applied sciences. The heavy demand for SANS is documented by the large over-booking factors at all neutron facilities. So, even in future we have to expect exciting results obtained by this method.

Appendices

A Further details about the correlation function

In this appendix we consider further details about the correlation function Γ. The first interesting property is the convolution theorem. In equation 5.21 it was stated that the correlation function in real space is a convolution while in reciprocal space the correlation function is a product (eq. 5.20). We simply calculate the Fourier transformation of $\Gamma(\mathbf{r})$:

$$\begin{aligned}
\Gamma(\mathbf{Q}) &= \mathcal{F}\left[\Gamma(\mathbf{r})\right] && (5.68)\\
&= \frac{1}{V}\int\limits_V d^3r \int\limits_V d^3r'\ \rho(\mathbf{r}+\mathbf{r}')\cdot\rho(\mathbf{r}')\cdot\exp(\mathrm{i}\mathbf{Q}\mathbf{r}) && (5.69)\\
&= \frac{1}{V}\int\limits_V d^3r \int\limits_V d^3r'\ \rho(\mathbf{r}+\mathbf{r}')\cdot\rho(\mathbf{r}')\cdot\exp(-\mathrm{i}\mathbf{Q}\mathbf{r}')\exp(\mathrm{i}\mathbf{Q}(\mathbf{r}'+\mathbf{r})) && (5.70)\\
&= \frac{1}{V}\int\limits_V d^3u\ \rho(\mathbf{u})\exp(-\mathrm{i}\mathbf{Q}\mathbf{u}) \int\limits_V d^3u'\ \rho(\mathbf{u}')\exp(\mathrm{i}\mathbf{Q}\mathbf{u}') && (5.71)\\
&= \frac{1}{V}\rho^*(\mathbf{Q})\rho(\mathbf{Q}) \qquad \text{with } \mathbf{u}=\mathbf{r}',\ \mathbf{u}'=\mathbf{r}'+\mathbf{r} && (5.72)
\end{aligned}$$

In line 5.70 we split the exponential according to the two arguments of the scattering length density. These variables are finally used for the integration. For extremely large volumes V the integration limits do not really matter and stay unchanged – otherwise surface effects would play a role. Finally we arrive at the already known product of the scattering amplitudes.

The overlap of two displaced spheres has a lens shape and is calculated as a spherical segment being proportional to the solid angle minus a cone. So the lens has the following volume:

$$\begin{aligned}
V_{\text{lens}} &= \frac{4\pi}{3}R^3\cdot 2\cdot\left(\frac{1}{4\pi}\int\limits_0^{2\pi} d\phi \int\limits_0^{\alpha} d\vartheta\ \sin\vartheta\ \ -\frac{1}{4}\cos\alpha\ \sin^2\alpha\right) && (5.73)\\
&= \frac{4\pi}{3}R^3\left(1-\frac{3}{2}\frac{r}{2R}+\frac{1}{2}\left(\frac{r}{2R}\right)^3\right) \qquad \text{with } \cos\alpha=\frac{r}{2R} && (5.74)
\end{aligned}$$

The displacement is given by r and the radius of the sphere is R. The result is finally used in equation 5.22.

The next topic aims at the real space correlation function with the model exponential decay in one dimension (eq. 5.24). We simply consider the variable z. The Fourier transformation is done in the following explicitly:

$$\Gamma(Q_z) = \int_{-\infty}^{\infty} dz \, \left(\left\langle \left(\rho - \langle\rho\rangle\right)^2 \right\rangle \exp\left(-|z|/\xi\right) + \langle\rho\rangle^2 \right) \exp(\mathrm{i}Q_z z) \tag{5.75}$$

$$= \left\langle \left(\rho - \langle\rho\rangle\right)^2 \right\rangle \cdot \frac{2\xi}{1+\xi^2 Q_z^2} \quad + \quad 2\pi\langle\rho\rangle^2 \delta(Q_z) \tag{5.76}$$

We obtain a product of the scattering length density fluctuations, a size of the correlation 'volume', and a Lorentz function which is typical for Ornstein-Zernicke correlation functions. A second addend appears due to the Q-independent term $\langle\rho\rangle^2$. Constants Forier-transform to delta functions which are infinitely sharp peaks at $Q = 0$. In the scattering experiment they are not observable. The same calculation can be done in three dimensions (with similar results):

$$\Gamma(\mathbf{Q}) = \left\langle \left(\rho - \langle\rho\rangle\right)^2 \right\rangle \cdot \int_V d^3r \, \exp\left(-|\mathbf{r}|/\xi\right) \exp(\mathrm{i}\mathbf{Q}\mathbf{r}) \quad + \quad \cdots \tag{5.77}$$

$$= \left\langle \left(\rho - \langle\rho\rangle\right)^2 \right\rangle \cdot \int_0^{2\pi} d\phi \int_0^{\pi} d\vartheta \, \sin\vartheta \int_0^{\infty} dr \, r^2 \, \exp\left(-r/\xi\right) \frac{\sin(Qr)}{Qr} \tag{5.78}$$

$$= \left\langle \left(\rho - \langle\rho\rangle\right)^2 \right\rangle \cdot 4\pi \cdot \frac{2\xi^3}{(1+\xi^2\mathbf{Q}^2)^2} \tag{5.79}$$

This functional form appears for polymer gels on large length scales. The density of the polymer network tends to fluctuations which are described by eq. 5.79. To make the looking of eq. 5.79 more similar to the Lorentz function the denominator is seen as a Taylor expansion which will be truncated after the Q^2 term. Then the Q-dependent term is $\Gamma(\mathbf{Q}) \sim (1 + 2\xi^2\mathbf{Q}^2)^{-1}$. Finally, we can state that the functional form of eq. 5.25 is 'always' obtained.

B Guinier Scattering

The crucial calculation of the Guinier scattering is done by a Taylor expansion of the logarithm of the macroscopic cross section for small scattering vectors Q. Due to symmetry considerations there are no linear terms, and the dominating term of the Q-dependence is calculated to be:

$$R_g^2 = -\frac{1}{2} \cdot \frac{\partial^2}{\partial Q^2} \ln\left(\rho(\mathbf{Q})\rho(-\mathbf{Q})\right)\Big|_{\mathbf{Q}=0} \tag{5.80}$$

$$= -\frac{1}{2} \cdot \frac{\partial}{\partial Q} \frac{2\Re\left(\rho(\mathbf{Q}) \int d^3r \, \rho(\mathbf{r})(-\mathrm{i}\mathbf{r}) \exp(-\mathrm{i}\mathbf{Q}\mathbf{r})\right)}{\rho(\mathbf{Q})\rho(-\mathbf{Q})}\Bigg|_{\mathbf{Q}=0} \tag{5.81}$$

$$
\begin{aligned}
&= -\Re\frac{\rho(\mathbf{Q})\int d^3r\ \rho(\mathbf{r})(-\mathbf{r}^2)\exp(-\mathrm{i}\mathbf{Q}\mathbf{r})}{\rho(\mathbf{Q})\rho(-\mathbf{Q})}\bigg|_{\mathbf{Q}=0} \\
&\quad -\Re\frac{\int d^3r\ \rho(\mathbf{r})(\mathrm{i}\mathbf{r})\exp(\mathrm{i}\mathbf{Q}\mathbf{r})\int d^3r\ \rho(\mathbf{r})(-\mathrm{i}\mathbf{r})\exp(-\mathrm{i}\mathbf{Q}\mathbf{r})}{\rho(\mathbf{Q})\rho(-\mathbf{Q})}\bigg|_{\mathbf{Q}=0} + 0 \qquad (5.82)\\
&= \langle\mathbf{r}^2\rangle - \langle\mathbf{r}\rangle^2 \qquad (5.83)\\
&= \left\langle\left(\mathbf{r}-\langle\mathbf{r}\rangle\right)^2\right\rangle \qquad (5.84)
\end{aligned}
$$

The first line 5.80 contains the definition of the Taylor coefficient. Then, the derivatives are calculated consequently. Finally, we arrive at terms containing the first and second momenta. The last line 5.84 rearranges the momenta in the sense of a variance. So the radius of gyration is the second moment of the scattering length density distribution with the center of 'gravity' being at the origin. We used the momenta in the following sense:

$$
\langle\mathbf{r}\rangle = \int d^3r\ \mathbf{r}\rho(\mathbf{r}) \Bigg/ \int d^3r\ \rho(\mathbf{r}) \qquad (5.85)
$$

$$
\langle\mathbf{r}^2\rangle = \int d^3r\ \mathbf{r}^2\rho(\mathbf{r}) \Bigg/ \int d^3r\ \rho(\mathbf{r}) \qquad (5.86)
$$

So far we assumed an isotropic scattering length density distribution. In general, for oriented anisotropic particles, the Guinier scattering law would read:

$$
\frac{d\Sigma}{d\Omega}(\mathbf{Q}\to 0) = \frac{d\Sigma}{d\Omega}(0)\cdot\exp\left(-Q_x^2\left\langle\left(x-\langle x\rangle\right)^2\right\rangle - Q_y^2\left\langle\left(y-\langle y\rangle\right)^2\right\rangle - Q_z^2\left\langle\left(z-\langle z\rangle\right)^2\right\rangle\right) \qquad (5.87)
$$

Here, we assumed a diagonal tensor of second moment. This expression allows for different widths of scattering patterns for the different directions. In reciprocal space large dimensions appear small and vice versa. Furthermore, we see that R_g is defined as the sum over all second momenta, and so in the isotropic case a factor $\frac{1}{3}$ appears in the original formula 5.35.

C Details about Scattering of Microemulsions

The first step for the derivation of the scattering formula for microemulsions takes place on the level of the free energy (and the order parameter). The overall free energy is an integral over the whole volume, and contains only second order of the order parameter. So the derivatives in expression 5.61 can be understood as an operator acting on the order parameter, and the overall free energy is a matrix element of this operator – like in quantum mechanics. The wave functions can now be tranferred to the momentum space, i.e. the reciprocal space:

$$
F_0\big(\phi(\mathbf{k})\big) = \int d^3k\ \phi^*(\mathbf{k})\big[c\mathbf{k}^4 + g_0\mathbf{k}^2 + \omega_2\big]\phi(\mathbf{k}) \qquad (5.88)
$$

Now the order parameter appears with its Fourier amplitudes $\phi(\mathbf{k})$ and the operator becomes a simple polynomial as a wavevector $\mathbf{k}$. So the operator takes a diagonal form, because different states are not mixed anymore. The macroscopic cross section for the scattering vector $\mathbf{Q}$ is simply the expected value of the corresponding Fourier amplitude $\phi(\mathbf{Q})$. The statistical physics simply consider all possible Fourier amplitudes:

$$\frac{d\Sigma}{d\Omega}(\mathbf{Q}) \propto \frac{\int d^n\phi(\mathbf{k})\ \phi^*(\mathbf{Q})\phi(\mathbf{Q}) \exp\left(-\frac{1}{k_BT}F_0\big(\phi(\mathbf{k})\big)\right)}{\int d^n\phi(\mathbf{k})\ \exp\left(-\frac{1}{k_BT}F_0\big(\phi(\mathbf{k})\big)\right)} \tag{5.89}$$

$$= -k_BT\frac{\partial}{\partial\omega_2}\ln\int d^2\phi(\mathbf{Q})\ \exp\left(-\frac{1}{k_BT}F_0\big(\phi(\mathbf{Q})\big)\right) \tag{5.90}$$

$$= -k_BT\frac{\partial}{\partial\omega_2}\ln\left(\frac{1}{\sqrt{\frac{1}{k_BT}(c\mathbf{Q}^4+g_0\mathbf{Q}^2+\omega_2)}}\right)^2 \tag{5.91}$$

$$= \frac{k_BT}{c\mathbf{Q}^4+g_0\mathbf{Q}^2+\omega_2} \quad \propto \quad \Gamma(\mathbf{Q}) \tag{5.92}$$

In line 5.90 the considered space of Fourier amplitudes has been reduced to the single important one. There are only two amplitudes left, which can be understood as the real and imaginary part of the complex amplitude. So the residual integral is 2-dimensional. The integral is Gaussian, and the result is known well. In line 5.91 the important dependencies are kept and all constant factors cancel out. The final result is the scattering function which is basically the reciprocal operator of line 5.88. This derivation is an explicit example of the fluctuation dissipation theorem.

To interpret the meaning of the scattering function the real space correlation function is calculated. While before the absolute value of the scattering intensity stayed rather undefined, in this representation absolute values have a meaning:

$$\Gamma(\mathbf{r}) = \left\langle\big(\rho-\langle\rho\rangle\big)^2\right\rangle\cdot\exp\big(-|\mathbf{r}|/\xi\big)\cdot\frac{\sin(kr)}{kr} \quad + \quad \langle\rho\rangle^2 \tag{5.93}$$

Furthermore the coefficients get a meaning: There is a correlation length ξ describing the decay of the correlations with the distance $\mathbf{r}$. The oscillating term describes the alternating appearance of oil and water domains. The domain spacing d is connected to the wavevector $k = 2\pi/d$. The connection to the original coefficients is given by:

$$k = \left[\frac{1}{2}\sqrt{\frac{\omega_2}{c}} - \frac{1}{4}\frac{g_0}{c}\right]^{\frac{1}{2}} \qquad \text{and} \qquad \xi = \left[\frac{1}{2}\sqrt{\frac{\omega_2}{c}} + \frac{1}{4}\frac{g_0}{c}\right]^{-\frac{1}{2}} \tag{5.94}$$

So the overall scattering formula takes the expression given in eq. 5.62. This example shows clearly that the real space correlation function supports the interpretation of scattering formulas obtained from a Landau approach with coefficients that are hard to connect to microscopic descriptions.

References

[1] R.-J. Roe, *Methods of X-ray and Neutron Scattering in Polymer Science* (Oxford University Press, New York, 2000).

[2] J.S. Higgins, H.C. Benoît, *Polymers and Neutron Scattering* (Clarendon Press, Oxford, 1994).

[3] J. Skov Pedersen, D. Posselt, K. Mortensen, *J. Appl. Cryst.* **23**, 321 (1990).

[4] O. Glatter, *J. Appl. Cryst.* **10**, 415 (1977).

[5] O. Glatter, *J. Appl. Cryst.* **12**, 166 (1979).

[6] T. Vad, W.F.C. Sager, J. Zhang, J. Buitenhuis, A. Radulescu, *J. Appl. Cryst.* **43**, 686 (2010).

[7] H. Endo, M. Mihailescu, M. Monkenbusch, J. Allgaier, G. Gompper, D. Richter, B. Jakobs, T. Sottmann, R. Strey, I. Grillo, *J. Chem. Phys.* **115**, 580 (2001).

[8] S. Gagliardi, V. Arrighi, R. Ferguson, A.C. Dagger, J.A. Semlyen, J.S. Higgins, *J. Chem. Phys.* **122**, 064904 (2005).

[9] H. Frielinghaus, D. Schwahn, L. Willner, *Macromolecules* **34**, 1751 (2001).

[10] H. Frielinghaus, D. Schwahn, K. Mortensen, K. Almdal, T. Springer, *Macromolecules* **29**, 3263 (1996).

[11] J.H. Lee, M.L. Ruegg, N.P.Balsara, Y. Zhu, S.P. Gido, R. Krishnamoorti, M.H. Kim *Macromolecules* **36**, 6537 (2003) and B.J. Reynolds, M.L. Ruegg, N.P. Balsara, C.J. Radke, T.D. Shaffer, M.Y. Lin, K.R. Shull, D.J. Lohse *Macromolecules* **37**, 7410 (2004)

[12] N.R. Washburn, T.P. Lodge, F.S. Bates *J. Phys. Chem. B* **104**, 6987 (2000)

[13] X. Ye, T. Narayanan, P. Tong, J.S. Huang, M.Y. Lin, B.L. Carvalho, L.J. Fetters, *Phys. Rev. E* **54**, 6500 (1996).

[14] S. Maccarrone, H. Frielinghaus, J. Allgaier, D. Richter, P. Lindner, *Langmuir* **23**, 9559 (2007).

[15] M. Teubner, R. Strey, *J. Chem. Phys.* **87**, 3195 (1987).

[16] Internal communication with M. Kraus, G. Goos, and G. Gompper; see also G. Gompper, M. Kraus, *Phys. Rev. E* **47**, 4301 (1993). and G. Gompper, G. Goos, *Phys. Rev. E* **50**, 1325 (1994).

[17] J. Haug, H. Kruth, M. Dubiel, H. Hofmeister, S. Haas, D. Tatchev, A. Hoell, *Nanotechnology* **20**, 505705 (2009).

[18] G. Goerigk, K. Huber, R. Schweins, *J. Chem. Phys.* **127**, 154908 (2007) and G. Goerigk, R. Schweins, K. Huber, M. Ballauff, *Europhys. Lett.* **66**, 331 (2004).

[19] P. Fischer, R. Zeller, G. Schütz, G. Goerigk, H.G. Haubold, *J. Phys. IV France* **7**, C2-753 (1997).

Exercises

E5.1 Fraunhofer far field for grating

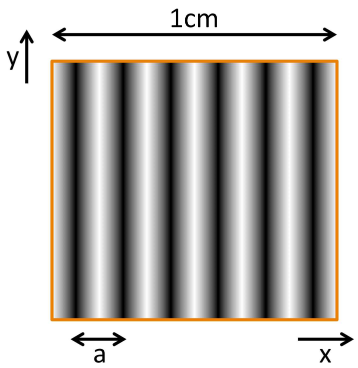

We consider a grating with a macroscopic area $1 \times 1\text{cm}^2$, and a mesoscopic periodicity of $a = 100\text{Å} = 10\text{nm}$. The edges of the grating should be soft. The transmission function is assumed to be: $T(x) = (1 + cos(\frac{2\pi}{a}x))/2$.

To which terms can the transmission function be divided?

☐ a) $\frac{1}{2}$ ☐ b) $\frac{1}{3}$ ☐ c) $\frac{1}{4}$

$\frac{1}{2}\exp(\mathrm{i}q_1 x)$ with

☐ a) $q_1 = \frac{2\pi}{a}$ ☐ b) $q_1 = \frac{4\pi}{a}$ ☐ c) $q_1 = \frac{\pi}{2a}$

$\frac{1}{2}\exp(\mathrm{i}q_2 x)$ with

☐ a) $q_2 = -\frac{2\pi}{a}$ ☐ b) $q_2 = -\frac{4\pi}{a}$ ☐ c) $q_2 = -\frac{\pi}{2a}$

To which kind of pattern do the three terms contribute?

☐ a) flat background ☐ b) primary beam ☐ c) no contribution

☐ a) slowly decaying function in the center of the pattern with a width of q_1
☐ b) many peaks at q_1, $2q_1$, $3q_1$, $4q_1$, ...
☐ c) single peak at q_1

☐ a) slowly decaying function in the center of the pattern with a width of q_2
☐ b) many peaks at q_2, $2q_2$, $3q_2$, $4q_2$, ...
☐ c) single peak at q_2

In the y-direction the grating does not show any structure.
To which kind of modulation does this correspond?

☐ a) constant ☐ b) $\exp(\mathrm{i}q_1 x)$ ☐ c) $\exp(\mathrm{i}q_2 x)$

What does this mean for the structure of the pattern on the detector?

☐ a) slowly decaying function in the center with a width of q_1
☐ b) sharp contours accordingly to the primary beam
☐ c) infinitely smeared out patterns in the y-direction

E5.2 The Pin-Hole Camera

The condition for the pinhole geometry is that the solid angle of the pin-hole observed from the position of the detector is equal or smaller than the solid angle of the object, here: the entrance aperture. Assume a symmetric SANS instrument with equal distances between the entrance aperture and the pin-hole (and sample), and between the pin-hole and the detector.

What is the ratio of the entrance aperture and the pin-hole dimensions?

☐ a) 2 ☐ b) 3 ☐ c) 4

What is the ratio of the areas?

☐ a) 2 ☐ b) 3 ☐ c) 4

Assume that the eye operated as a pin-hole camera. The sizes may be for the aperture 1mm, for the retina distance 2cm, and for the object 1km.

What would be the minimal object size that could be resolved at this distance?

☐ a) 10m ☐ b) 50m ☐ c) 200m

Why do we see better?

☐ a) aperture smaller ☐ b) eye contains lens ☐ c) we do not see better

E5.3 Understanding of the Manuscript

The correlation function for a microemulsion is given in real space by eq. 5.93 and in reciprocal space by eq. 5.62. They describe an oscillating structure with the wavevector k and a correlation length ξ. A simpler correlation function is already obtained by equations 5.24 (real space) and 5.79 (reciprocal space, exact formula). Here, only a decaying correlation function is assumed in real space.

Which value does the k-vector of the first case take to obtain identical results?

☐ a) $k = \infty$ ☐ b) $k = \xi^{-1}$ ☐ c) $k = 0$

In the structure factor of spherical colloids, the double radius $2R$ occurs for the simplest approximation in the effective concentration and the Q-dependent term $K(Q, 2R)$ (see eq. 5.56).

Why does the double radius occur in this description?

☐ a) Here, only two colloids are considered. For three colloids $3R$ would appear.
☐ b) The closest distance of two colloids is $2R$.
☐ c) The square of the amplitude arising in the intensity causes effectively a factor 2.

The Porod behaviour (see eq. 5.34) and the high-Q limit of a polymer (see eq. 5.50) are simple power laws Q^α with α being -4 and -2 in the first and second case.

What do these power laws indicate?

☐ a) The exponent indicates how sharp the effective particle is defined at its surface.
☐ b) The dimensionality (3 for sphere, 1 for polymer) plus 1 directly determines α.
☐ c) Self-similarity. The structure looks on different length scales identical.

E5.4 Contrast Variation Experiment on Micelles

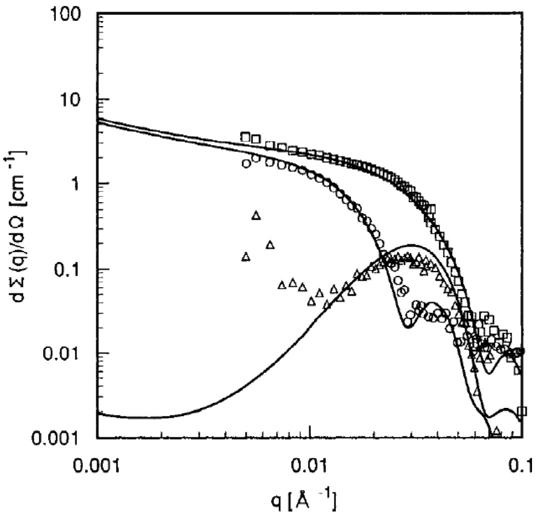

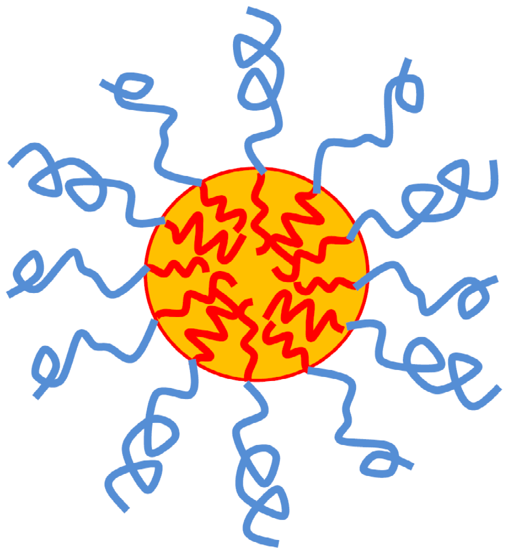

The three symbols □, ○, and △ indicate the characteristic small angle scattering of spherical polymer micelles under different important contrast conditions. There are three conditions called: *shell contrast*, *core contrast* and *zero average contrast*. The *shell contrast* highlights the shell of the micelle (being hydrogenated) while the rest is deuterated. The *core contrast* highlights the core of the micelle (being hydrogenated) while the rest is deuterated. For the *zero average contrast* the average contrast of the deuterated core and the hydrogenated shell matches with the solvent.

Which condition can be connected to which symbol (or curve)?

□ a) △-shell ○-core □-zero □ b) ○-shell □-core △-zero □ c) □-shell △-core ○-zero

Why?

E5.5 Spherical Form Factor

In microemulsions the topology of spherical droplets is quite frequent. We would like to assume a deuterated oil droplet of radius R surrounded by the protonated surfactant film and normal water (H_2O). For simplicity, the oil is assumed to be homogenous with a scattering length density ρ, and the surrounding materials are assumed to have an average zero scattering length density (which is nearly true). So the amplitude $\rho(Q)$ is calculated by the Fourier transform of a homogenous sphere. The macroscopic scattering cross section is normalized to the overall volume.

Calculate the three dimensional Fourier transformation of a solid sphere. Use spherical coordinates, and integrate in the order ϕ, ϑ, r. What is the simplicity of the integral over ϕ? How can the integral over ϑ be simplified (what is the variable X)? What does the kernel of the integral mean before the integration over r is performed? How would the integral be generalized for a scattering length density profile $\rho(r)$ with spherical symmetry? What is the meaning of the term $\sin(Qr)/(Qr)$?

The formulas 5.28 to 5.33 already show the solution of the problem. Nonetheless, the student should be motivated to rationalize each step of the derivation. The highly motivated student might also derive the sphere scattering from eq. 5.22.

I thank my family and all my colleagues for supporting this SANS-script.